Non-linear Analysis of Orthotropic Composite Slabs in Fire

Xinmeng Yu[a *], Zhaohui Huang[a], Ian Burgess[a], Roger Plank[b]

[a] Department of Civil and Structural Engineering, The University of Sheffield , Sheffield S1 3JD, UK

[b] School of Architectural Studies, The University of Sheffield, Sheffield S10 2TN, UK

ABSTRACT

In this study an orthotropic slab finite element is developed to model orthotropic slabs in fire, using a layered 9-noded iso-parametric slab element and a 3-noded beam element. The element is assembled from a solid slab element which represents the continuous upper portion of the profile, and a special beam element which represents the ribbed lower portion. An equivalent width for the cross-section of this beam element is determined according to the dimensions of the solid slab element and the cross-section of the ribbed profile, and the beam shares the nodes of the solid slab element. The temperature within each layer of the slab element can vary between adjacent Gauss integration points so as to reflect temperature variations in the horizontal plane. Several fire tests on composite slabs have been modelled to validate the approach. Cases of orthotropic slabs with wide range of parameters defining the ribbed profile have been studied, which show that the orthotropic slab model is robust and effective in reflecting the influence of the shape of ribs on the thermal and structural performance of the slabs in fire. The study shows the influence of decking shape on the thermal and structural behaviours of orthotropic slabs. A simple evaluation method for profile selection is proposed.

Keywords: Orthotropic slabs; Composite structures; Fire resistance; Decking shapes, Numerical modelling

---

* Corresponding author: Tel: +44 114 222 5362; Fax: +44 114 222 5700
E-mail address: x.m.yu@sheffield.ac.uk

NOTATION

The geometric parameters defining the decking may be referred to Fig. 1:

h	Slab depth
H_{eff}	Effective depth of an orthotropic slab (defined in EN 1994-1-2:2005(E), Annex D)
H_s	Depth of concrete slab (continuous upper portion)
H_r	Depth of rib (height of steel decking)
L	Wave-length of the decking profile
L_0	Average of L_1 and L_2
L_1	Distance between two upper flanges
L_2	Width of the lower flange
L_3	Width of the upper flange
RWR	Rib width ratio $= L_0/(L_1+L_3)$
RDF	Rib depth factor = Depth of rib (mm) / 100 (mm)
α	Angle between lower flange and web of decking
A45	α=45º; similarly for A90, A120, *etc.*
$EC4_{eff}$	A slab in its effective depth , H_{eff}
P_h	Reinforcement position in the symmetry axis across the thinner part of the slab
P_c	Reinforcement position in the symmetry axis across the thicker part of the slab
T_h	Temperature at P_h
T_c	Temperature at P_c
T_{ec4}	Reinforcement temperature of an orthotropic slab at its effective depth
ϕ_{tf}	View factor at top flange of the decking
ϕ_{web}	View factor at web of the decking
NWC	Normal-weight concrete
LWC	Light-weight concrete

Non-linear Analysis of Orthotropic Composite Slabs in Fire

Xinmeng Yu, Zhaohui Huang, Ian Burgess, Roger Plank

1. INTRODUCTION

Orthotropic metal-decked composite slabs have been widely used in recent decades. These composite slabs consist of a cold-formed profiled thin-walled (typically, 0.6-1.2mm) steel decking, and concrete which is cast on top of this. Normally, the concrete is reinforced with a light anti-crack mesh, and may also contain individual bars, usually placed within the ribs. The profiles can be classified into trapezoidal and re-entrant types. Trapezoidal decking may occasionally be used over long spans using extra-deep ribs which contain individual bars. However, the decking acts as reinforcement, being bonded to the slab surface through indentations in the profile, and the composite slab itself has a very low centre of reinforcement compared to a conventionally reinforced slab. Due to the intrinsic efficiency of composite construction and the displacement of concrete by the profile shape, considerably less concrete is used than in conventional reinforced concrete slab construction [1]. Another advantage of an orthotropic slab over a flat one is that it saves construction time since the decking is a permanent formwork which does not require propping. Trapezoidal decking slabs are more popular than re-entrant ones because of the relative ease of casting of concrete.

When the concrete is subjected to heating, there are distinct temperatures at which: (a) the free water is vaporised as steam, (b) the chemically bound water in the cement gel is released by dehydration into the liquid phase as free water, which subsequently vaporises. The water phase (bound, liquid or gaseous), the dimensions of the structure, the mixture type, concrete porosity and the heating history all affect the temperatures in the slab [2, 3]. An added complexity comes from the coupled thermo-hydral-mechanical processes in the heated concrete. It is obvious that modelling of heat and mass transfer within concrete in fire is very complicated. In fact, in Eurocode 4, the thermal properties are treated in a very simple way. In this study, for simplicity, Huang's model [4] is adopted to predict temperature distribution within the cross section of the composite slab. In this model, the moisture evaporation in the concrete and the specific heat and thermal conductivity properties of concrete and steel are considered as temperature-dependent. This is good enough for civil and structural engineering analyses.

Thermal analyses show that, when an orthotropic slab is subjected to fire attack, the temperature within its continuous upper portion varies in the horizontal plane due to the

presence of the ribs. The thinner part is subject to higher temperatures than the thicker part. The Cardington fire tests [5] showed that reinforcement temperatures in the thinner portions were much higher than in the thicker portions. This issue should be taken into account in the development of orthotropic slab model to analyse ribbed slabs in fire.

In Eurocode 4 [6] (EC4), orthotropic slabs may be treated as equivalent solid slabs with an effective depth (H_{eff}), and the steel decking is ignored in fire conditions. This method is not applicable to deep-deck slabs with rebar in the ribs. For these slabs, the fire resistance is usually expressed in standard classes, ranging from 30 to 120 minutes (and beyond) in 30-minute intervals. Only exposure from below is considered, which in practical cases will always be decisive. These rules are "highly empirical in nature, and lack a fundamental scientific basis" [7]. As stated above, the presence of the ribs makes orthotropic slabs different from flat ones in both their thermal and structural behaviour.

A number of models have been developed for modelling of orthotropic composite slabs in fire. In the first phase of an ECSC research project [7], a special-purpose model was developed for simulation of the mechanical behaviour of fire-exposed composite slabs. In order to obtain reasonable agreement between numerical and experimental results for the continuous decking slab, a full continuous horizontal crack separating the ribs from the concrete plane was assumed and explicitly taken into account. This was done simply by ignoring the contribution of the ribs and the steel decking to the stiffness.

Elghazouli and Izzuddin [8] developed a model in which the composite slab was treated as an orthogonal elasto-plastic grillage of beam-column elements, and temperature variations were introduced across the two orthogonal cross-section directions as well as along the element length. The deflections were obtained from the integration of the orthogonal beam-column elements. The shortcoming of this type of grillage model is that the realistic slab behaviour cannot be modelled properly in this way, since the effects of in-plane shear and Poisson's Ratio are ignored. This implies that tensile membrane action, which may cause a considerable reduction of displacements [9] of slabs deforming in double-curvature due to two-way support conditions, cannot be modelled.

Gillie *et al.* [10] described a method of modelling composite floor slabs using a stress-resultant approach. This approach combined the material behaviour and geometry of a plate into one set of equations. The internal membrane forces and moments per unit width of plate were calculated based on the strain, curvature and temperature of the plate reference surface. The set of stress resultants are two normal membrane forces, an in-plane shear force,

two bending moments and a twisting moment. In this model an unrealistic concrete material model was employed in which concrete was treated as elastic-perfectly plastic material. Another drawback of this method is that the model does not allow stresses within the slabs to be output from the analysis.

In the University of Sheffield's software, *Vulcan,* an effective-stiffness model [11] was developed in which the orthotropic slab was treated as a solid slab with different orthogonal stiffnesses and layered temperatures which are uniformly distributed horizontally. In this method the nominal thickness of the slab is from the top surface to the bottom level of the ribs. The effective-stiffness factors obtained from cross-sectional bending stiffnesses at ambient temperature are applied as constants to modify the material stiffness of the layered concrete slab throughout the fire duration. In reality, the effective-stiffness factors will change at elevated temperatures, due to the degradation of the material properties as temperature distributions change.

In Lim *et al.*'s model [12, 13], the solid part of the ribbed slab was modelled as an assembly of brick-like shell elements (Fig. 2a), and each individual rib was modelled using beam elements. The beam element was modelled in two parts, with concrete and steel properties in the lower part and non-load-bearing properties in the upper part. It is obvious that a large number of elements are needed for modelling composite slabs of practical dimensions in this way, and computation is extremely expensive. It is difficult for this approach to model certain types of decking slab which have very shallow indents, as shown in Fig. 2b.

The main objectives of this study are:

(1) To develop a more robust and flexible procedure for modelling of orthotropic composite decking slabs subject to fire conditions. One of the most important developments is to apply realistic temperature distributions within the decking slabs, especially the different representation of temperatures of the steel mesh within the thick and thin cross-sections of the slabs.

(2) To perform a series of numerical studies to investigate the thermal and structural behaviour of the most commonly-used composite decking slabs currently in use in the construction industry.

2. NON-LINEAR PROCEDURE FOR MODELLING OF ORTHOTROPIC COMPOSITE SLABS

2.1 The Orthotropic slab element

The software *Vulcan* has been developed at the University of Sheffield for three-dimensional analysis of composite and steel-framed buildings in fire. The program is based on a 3D non-linear finite element procedure in which a composite building is modelled as an assembly of beam-column, spring, shear connector and slab elements. The beam-column line element is three-noded, and its cross-section is divided into a matrix of segments, or fibres, to allow for variation of temperature, stress and strain through the cross-section [14]. Slabs are modelled using nine-noded layered plate elements based on Mindlin-Reissner theory, in which each layer can have different temperature and material properties [9]. Both material and geometric non-linearities are considered in beam-column and slab elements.

As shown in Fig. 3, the current orthotropic slab element is based on the pre-existing beam and solid slab elements in *Vulcan*. The element is assembled from a solid slab element, which represents the continuous upper portion of the profile, and an equivalent special beam element which represents the ribbed lower portion. It is assumed that the reference axis of the beam element coincides with the mid-plane of the slab element. An equivalent width for the cross-section of this beam element is determined according to the cross-sectional dimensions of the ribbed slab, and it shares the 3 middle nodes of the solid slab element on the reference plane. The previous non-linear formulations of both the solid slab and beam elements are employed. For slab elements, degraded stiffness is assembled at nine Gauss integration points according to the degradation status. Membrane locking is not an issue for thick composite slab elements. To mitigate shear locking, a reduced integration rule is used for the quadratic beam element. One important development in the current model, which differs from the previous model [9], is that the temperature of each layer of a slab element is not necessarily uniform in the horizontal plane, and it is assumed that the temperature can be varied between adjacent Gauss integration points. Therefore, realistic temperature distributions within the slabs can be represented by the current model. The cross-section of the beam element uses its segmented nature to represent different temperatures and materials within the ribs. In this model the beam element is normally used to represent a group of ribs of the composite slab, rather than just a single rib, and hence the width of the beam element is an equivalent width calculated from the *Rib Width Ratio* (RWR), a proportion of the width of

the solid slab element. It is therefore reasonable to assume that the beam element has only uniaxial properties, without significant torsional resistance.

The stiffness matrix of an orthotropic slab element $\mathbf{K}_{orth}$ is assembled from the stiffness matrices of a nine-noded solid slab element $\mathbf{K}_{slab}$ and a three-noded beam element $\mathbf{K}_{beam}$:

$$\mathbf{K}_{orth} = \mathbf{K}_{slab} + \mathbf{K}_{beam} \tag{1}$$

The slab element tangent stiffness matrix, $\mathbf{K}_{slab}$, is composed of the usual small-displacement stiffness matrix, the large-displacement stiffness matrix, and the stress level dependent geometric matrix. The detailed formulations can be found in Reference [9]. The beam elements, which represent the ribs below the continuous, thinner portion of the slab, share the three middle nodes of the upper slab elements, and it is assumed that they are fully attached (see Fig. 3). For the beam element the tangent stiffness matrix is composed of linear and non-linear stiffness matrices specified in Reference [14]. In this study the beam element represents a group of ribs of the composite slab, and hence the width of the beam element is an equivalent width calculated from the rib width as a proportion of the width of the solid slab element (see Fig. 3). As stated above, it is assumed that the beam element has only uniaxial properties, without torsional resistance. Hence the material constitutive matrix for the beam element can be represented as

$$\mathbf{D}' = \begin{bmatrix} E_t & 0 & 0 \\ 0 & 0 & 0 \\ 0 & 0 & 0 \end{bmatrix} \tag{2}$$

where E_t is the tangent modulus of the material.

The internal forces of the orthotropic slab element is obtained from the total of the solid slab element and the equivalent beam element. The detailed formulations can be found in References [9] and [14], respectively.

2.2 The simplified temperature distribution within each layer of the solid slab element

Due to the presence of the ribs, the temperature distribution within any layer of the solid slab element is non-uniform. In order to take this factor into account within the model a simplifying assumption has been made; the temperatures within a layer are divided into two zones, (hotter and cooler zones) at the Gauss integration points (see Fig. 4). The higher

temperatures at the thin parts of the slab (see Line 2 of Fig. 1) are defined at six Gauss integration points (1, 2, 3, 7, 8, 9), and the cooler temperatures at the thick part (see Line 1 of Fig. 1) are assigned to three Gauss integration points (4, 5, 6). The temperature distribution within the rib part is used to represent the temperature distribution of the cross-section of the beam element. This is a reasonable representation of the real temperature distribution within a ribbed slab (see Fig. 5). Hence, at each Gauss Integration Point, the material stiffness, strength, and thermal expansion are calculated according to the corresponding temperature.

3. MODEL VALIDATION

3.1 TNO fire test on a one-way simply supported slab

A major fire test was carried out at TNO in the Netherlands in September 1996 as part of an ECSC research project [1]. The test specimen consisted of a single span of slab with two Rectangular Hollow Section edge beams. The test specimen was 5.6m long x 4.6m wide, the beams spanning in the shorter distance. The test load was typical of normal office loading (imposed test load $3.55 kN/m^2$, self weight $3.10 kN/m^2$). The depth of the normal-weight concrete slab was 290mm, with A192 mesh (Φ6) positioned in such a way that the distance from the centre of the longitudinal bars to the unexposed face was 20mm. A 25mm diameter rebar was placed in each of the ribs. The constructional details are shown in Fig. 6. The compressive strength of the concrete was $49.5 N/mm^2$. The structural steel strengths were $409 N/mm^2$ for the hollow section and $349 N/mm^2$ for the plate, respectively, in the edge beams. The slab was unrestrained against thermal expansion, and the 200mm x 100mm RHS edge beams were restrained against rotation at both ends. The edge beams were designed to achieve at least 60 minutes' fire resistance, and the composite slab was reinforced to achieve 120 minutes' fire resistance. In order to gain information on the fire resistance of the slab, the beam was prevented from collapsing completely by blockwork pillars within the furnace, the tops of which were positioned 200mm below the beams. In this numerical study, the test load and the tested material properties of structural steel, concrete and reinforcement were used. Further details are available from Reference [1]. Before modelling the test, a thermal analysis was conducted to predict the temperature distributions within the cross-sections of the beams and ribbed slabs using *Vulcan*. Fig. 7 shows the comparison between predicted and tested temperatures at some key positions within the cross-sections of the beams and ribbed slabs. It is evident that very good agreement was achieved. These temperature predictions were used in the structural analysis.

Fig. 8 compares the predicted deflections using the current model and the previous effective-stiffness model at two key positions P1 and P2 (see Fig. 6), together with the test results. It can be seen that the curves predicted by the current model agree well with test results up to 70 minutes into the test. It is evident that the structural behaviour predicted by the two models differs beyond this point.

3.2 BRANZ fire test on a two-way simply supported slab

A series of full-scale fire tests conducted at the Cardington in the UK have shown that the fire resistance of unprotected composite floor structures is much better than standard furnace fire testing suggests. The composite concrete slabs may play an important role in increasing the fire resistance of the structure due to tensile membrane action, and so it is important to model the composite slabs correctly. Recently, six two-way simply supported concrete slabs subjected to the ISO834 fire curve were tested at the BRANZ fire test furnace in New Zealand. One of the tests, carried out on the 1st July 2002 [15], was on a Hibond orthotropic ribbed slab. The tested slab had the dimensions 4300x3300x130mm, measuring 4150mm by 3150mm between supports, and was made of normal-weight concrete with 30MPa compressive strength. The D147 reinforcement mesh ($198mm^2/m$, Φ8.7) was cold-worked with a yield strength of 565MPa placed at 20mm above the decking. The slab was subject to a uniformly distributed live load of $3.0\,kN/m^2$ during the fire test. The self weight was $2.47\,kN/m^2$.

A thermal analysis was performed using *Vulcan* to predict the temperature distributions within the cross-section of the slabs. Fig. 9 shows the comparisons of some predicted and tested key temperatures from bottom to top of the cross-section of the tested slabs. It is clear that a reasonable agreement was obtained, and the predicted temperatures were used in the structural modelling.

Fig. 10 shows a comparison of the central deflections predicted by the current orthotropic model and two other models with test results. The result predict by current model is closer to the test data than that predicted by Lim's model [13] before 120 minutes of fire, but the latter is closer to the test data beyond this fire stage. In the effective stiffness model the average temperatures layer-by-layer between the thinner and thicker parts were applied because this model assumes uniform temperatures for each layer. Reasonable agreement was achieved by the current and effective stiffness models with the test results up to 130 minutes in the test. Beyond this point the test deflections accelerated, while the predictions by both models were more stable. The reason for this difference between test and prediction may be due to the

large cracks which formed in the middle of the test slab. Certain observations made during the test [15] support this. Flames were seen to penetrate through the discrete crack in the middle of the slab at a late stage of the test, and significant corner cracking was observed.

3.3 Modelling full-scale fire test - Cardington Test 7

To study global structural and thermal behaviour, a full-scale fire test was conducted on the 4th floor of the eight-storey steel framed building at the Building Research Establishment's Cardington laboratory in January 2003 [16, 17]. The fire compartment was 11m long by 7m wide (Fig. 11). The building had been designed for a dead load of 3.65kN/m^2 and an imposed load of 3.5kN/m^2. Sandbags each of 1.1 tonne were applied over an area of 18m by 10.5m, spaced so that a uniform live loading of 3.05kN/m^2 was simulated for the fire test [16]. The exposed structure consisted of two secondary beams (305x165x40UB) of nominally S275 steel (of measured f_y=303MPa), an edge beam (356x171x51UB), two primary beams (356x171x51UB), nominally S350 (measured f_y=396MPa), and four columns (internal column sections were 305x305x198UC and external column sections were 305x305x137UC, of S350 steel). The overall depth of the slab was 130mm with rib depth 60mm, with A142 mesh 15mm above the decking. The profile of the decking can be obtained from Reference [8]. The compressive strength of the concrete was 37.01MPa. The yield strength of the reinforcement was 460MPa.

It was observed [18] that, after the fire test had finished and the structure had cooled, the composite slab had extensive cracking in both the longitudinal and transverse directions, though it cannot be stated definitively that this happened entirely during the heating phase. The main longitudinal crack was off-centre of the bay of the column grid. The main longitudinal and transverse cracks penetrated the full depth of the slab, and the longitudinal crack was 90mm wide near to their intersection. This extent of rupture seems unusual without a complete failure of the slab, but it can be seen that the ends of the reinforcing bars in two sheets of mesh had slipped relative to one another across the crack. This was clearly due to inadequate overlap of the adjacent sheets of mesh during construction of the building, so that only "fingers" of undeformed bars were overlapping, and that the anchorage which might have been achieved by overlapping the welds to the orthogonal reinforcement was not achieved. This situation would also have dictated the location of the longitudinal crack.

In order to model this inadequate overlapping of the mesh, three cases (Cases I, II, III) were modelled by reducing the strength of the reinforcement in this area by ¾, ½, and ¼

respectively. Thermal analysis was also conducted to obtain the temperature distribution within the cross section of the slabs. Fig. 12 shows both tested and predicted temperature distributions at some key positions within the cross-section of the slabs. The predicted temperature distribution in the slab, and the tested temperatures of the beams (in which the maximum temperature was 1000°C at 60 min test time), together with the material properties and loads detailed above, were applied to model the structural behaviour in the test. The predicted deflections at key position P1 (see Fig. 11) are shown in Fig. 13 for three different cases, together with the test results. It is evident that Case I had the most effective prediction up to 60 minutes of the test. In the cooling phase, the current model predicted less deflection than the test result. This is almost certainly due to the localised failure (the large ruptures) of the concrete slabs which happened during cooling stage. The current model cannot handle localisation of failure of concrete slabs. However, the accuracy of the current model's predictions is reasonably good considering the complexity of such a large-scale fire test.

4. THE INFLUENCE OF RIB SHAPES OF DECKING SLABS IN FIRE: A PARAMETRIC STUDY

4.1 Decking shape parameters

Reference [7] lists a number of decking types with trapezoidal and re-entrant profiles. These different decking types have been re-sorted and grouped according to the depths (H_r) and average widths (L_0) of their ribs. Considering the popularity and the rib width ratio (RWR) of existing profiles, in this study the 7 groups shown in Fig. 14 have been used to carry out the parametric study. The parameters of these groups are listed in Table 1.

When an orthotropic slab is subjected to fire, the heat flux due to radiation which acts on the bottom surface of the decking differs with profile shape and distance. The View Factor is used to quantify this relationship. In this study, a simplified model has been adopted to address this factor as follows:

(1) Unit view factor is assumed at bottom of the rib, as the reference level.

(2) The view factors at the top flange (ϕ_{tf}) and web (ϕ_{web}) of the indented surfaces of the slab were assumed to be uniform and determined according to Fig. 15. This approximation was developed by Wickström *et al.* [19] in 1990 and subsequently accepted by EC4.

(3) The view factors stay constant throughout the fire stage.

4.2 Thermal and structural behaviour of profiled slabs

A two-way simply supported 9m x 6m composite floor with a secondary beam placed in the middle of the shorter span (see Fig. 16) subject to ISO834 fire was selected for this study. This dimension is similar to those used in Cardington fire tests. The secondary beam was assumed to be protected so that the bottom flange and web temperatures linearly increased to 620°C at 180 minutes. This secondary beam is protected for the purpose of large-displacement comparison because slabs of some groups can not last long in fire without the secondary beam being protected. The thickness of the continuous thinner portion was 70mm, with A142 mesh located 20mm above the top flange of the decking. The uniformly distributed load was assumed as 5kN/mm^2. The compressive strengths of both normal-weight concrete (NWC) and light-weight concrete (LWC) at ambient temperature were 30N/mm^2. Only a quarter of the structure was analysed due to the inherent symmetry of the slab. The study focused on the influence of the decking shape on the thermal and structural behaviours of the composite floor in fire.

The thermal analyses were conducted using *Vulcan,* again based on Huang's model [4], and the structural behaviour was predicted by the model developed in this paper. In this study 80 cases (see Table 1) were modelled for both NWC and LWC, including slabs ($EC4_{eff}$) treated as solid with nominal effective thicknesses (H_{eff}) obtained according to Eurocode 4. In order to present the results more effectively all notations used in the following figures are defined in the Notation section.

Figs. 17 and 18 show the temperatures of reinforcing steel at the thicker and thinner sections (T_c and T_h) of NWC and LWC slabs, respectively, for various groups with α=90º (A90). In order to save space here, only the influence of decking shapes on the reinforcement temperatures of LWC slabs of various groups are shown in Fig. 19. After analysing the results, some general conclusions about the temperatures of reinforcement within the cross-sections of different decking slabs can be drawn as follows:

- The influence of rib shape on the reinforcement temperature is not very significant. However, the effects on the LWC slabs are more significant than on NWC slabs.
- Generally speaking, T_c decreases with increase of RWR, but the depth of the rib also influences the temperature; this makes the T_c values in Group 7 higher than those in Group 6 (see Figs. 17a and 18a). The difference of T_h between different groups is not very great.

- The influence of the angle α on T_c decreases with RWR, from more than 15% (based on A90) for Groups 1 and 2 to less than 5% for Group 7. The effect on T_h is the reverse.
- For the slabs with RWR $\leq$ 0.32 (Groups 1-3), the shape of the rib has little influence on T_h, but considerably influences T_c. The greater the angle α, the lower T_c becomes. Deeper ribs (with greater H_r) also affect the influence of the angle α on T_c. For those with RWR over 0.6 (Groups 4-7) the shape of rib does not influence T_c very much, especially when α is between 60^o and 105^o.
- After 180min of the ISO834 fire, for NWC slabs with 90º rib angle, T_h is in the range 650ºC-750ºC and T_c in the range 450ºC-700ºC. For LWC slabs with 90º rib angle, T_h is in the range 650ºC-700ºC and T_c in the range 350ºC-650ºC.
- If a profiled slab is treated as solid, with an effective thickness obtained according to EC4, the reinforcing mesh temperature obtained from thermal analysis is close to T_c. This gives the slab a better fire resistance than the real ribbed slab, especially in the later stages of the fire.

Figs. 20 and 21 show comparisons of the deflections at Position A (see Fig. 16) among the seven groups of profiled NWC and LWC slabs, respectively. Detailed comparisons of deflection with the rib angle within each group are shown in Figs. 22. Again, to save space, only the results for LWC are shown. From results obtained, some general conclusions concerning the structural behaviour of composite slabs in fire can be drawn.

Deflections using the EC4 assumption, which defines an effective flat slab and a tabulated temperature distribution at standard fire resistance ratings, are always on the unsafe (low) side compared with those modelled by the current process, except for Group 1. If the likelihood of localised failure is taken into consideration, $EC4_{eff}$ is even less conservative.

Given the Eurocode definitions of the thermal properties of concrete, LWC slabs give better thermal performance than NWC slabs with the same compressive strength. The rib angle α has less influence on LWC slabs than on NWC slabs, and the influence of α decreases with increasing RWR. The influence of the rib angle on LWC slab deflections is within 20% (based on A90). Comparing the predicted deflections using $EC4_{eff}$ and the current model, closer results were obtained for NWC slabs than for LWC ones. The influence of α decreases with increasing RWR, but increases with the rib depth.

- In common with its influence on temperatures, the influence of the rib shape on the structural performance is not very significant. In each group, the slab with $\alpha = 90^{o}$ has higher deflection than those with other angles. This means that it is reasonable to assume $\alpha = 90^{o}$ as a conservative assumption when evaluating the fire resistance of an orthotropic slab.
- Considering Figs. 20 and 21 in detail, it is evident that the Groups 5 and 6 have better fire resistance than Groups 3, 4 and 7, which in turn have better fire resistance than Groups 1 and 2. It is interesting that the relative fire resistance level of slabs can be evaluated roughly by the summation of the RWR and the *Rib Depth Factor* (RDF, the depth of rib divided by 100). The fire resistance level of the slab increases with (RWR + RDF), as shown in Table 2, in which Classes A, B and C correspond to fire resistance levels (A>B>C). These dimensionless values can be interpreted in general terms; given the same slab thickness (in the continuous portion) and material properties, the greater the value the better the fire resistance. However the fire resistance of a slab also depends on the thickness, the load, the boundary conditions, material properties, *etc*., so we can not relate these values to hours of fire resistance directly.

5. CONCLUSIONS

In this paper the development of orthotropic slab model to model ribbed slabs in fire has been described. The model has been developed from the slab and beam element formulations contained within the software *Vulcan* developed at the University of Sheffield. The two main new features of the model are:

(1) The continuous top part of the ribbed slab is represented by solid slab elements, and the lower (rib) part is modelled as an equivalent beam element with uniaxial properties. Both the orthotropic character and membrane actions of ribbed slabs are taken into account in a logical manner. This approach also allows the modelling of deep-deck slabs.

(2) The model allows non-uniform temperature distribution within each layer of the solid slab element. Hence, the temperature distributions across the cross-section of the profiled slabs can be represented more accurately than in uniform-thickness layered shell elements. This overcomes the drawbacks of the previous effective-stiffness model, in which uniform average layer temperatures are used. In particular, a better

representation of reinforcement temperatures across the thin and thick sections of the ribbed slab is achieved by the current model.

A series of parametric studies using various decking shapes have been carried out. By representing the hotter and cooler temperatures in the thinner and thicker portions of the slab, it can be seen that the current model can sensitively reflect the influence of shape on the thermal and structural behaviours. It also shows that the Simplified Method in EC4, which treats the orthotropic slab as an equivalent solid slab with an effective thickness, is not sufficiently conservative, especially in the later stages of a fire. LWC slabs have better fire performance than NWC ones. When considering the choice of suitable decking profiles for orthotropic slabs in construction, a simple calculation (Table 2) can be used as an alternative method for approximate evaluation of the fire resistance level.

REFERENCES

[1] *Corus Construction Centre* website: http://www.corusconstruction.com.

[2] Bazant, Z.P. and Kaplan, M., "*Concrete at high temperatures"*, Longman Group Limited, 1996, (ISBN 0-582-08626-4).

[3] Tenchev, R.T., Li, L.Y., Purkiss, J.A. and Khalafallah, B.H., "Finite element analysis of coupled heat and mass transfer in concrete when it is in a fire", *Magazine of Concrete Research,* **53** (2), (2001) pp117-125.

[4] Huang, Z., Platten, A., and Roberts, J. "Non-linear finite element model to predict temperature histories within reinforced concrete in fires*"*, *Building and Environment*, 31(2) (1996), pp 109-118.

[5] Bentley P.K., Shaw D., and Tomlinson L., *"ECSC Project: Behaviour of a Multi-Storey Steel-Framed Building Subjected to Natural Fires. Test 2: Plane Frame Data Files: Temperature Measurements",* Report S423/2/Part T1-T2, Swinden Technology Centre, British Steel plc, South Yorkshire, UK, 1996.

[6] European Committee for Standardisation, "*prEN1994-1-2: Eurocode 4 - Design of composite steel and concrete structures"*, Final Draft (Stage 34), CEN, Brussels, 2003.

[7] Both, C., "*The fire resistance of composite steel-concrete slabs"*, PhD thesis, TU Delft, Delft University Press, 1998, (ISBN 90-407-1803-2-Y).

[8] Elghazouli, A.Y. and Izzuddin, B.A., "Analytical assessment of the structural performance of composite floors subject to compartment fires", *Fire Safety Journal,* **36,** (2001) pp769-793.

[9] Huang, Z., Burgess, I.W. and Plank, R.J., "Modelling membrane action of concrete slabs in composite buildings in fire - Part I: Theoretical development", *Journal of Structural Engineering, ASCE,* **129** (8) (2003) pp1093-1102.

[10] Gillie, M., Usmani, A., Rotter, M. and O'Connor, M., "Modelling of heated composite floor slabs with reference to the Cardington experiments", *Fire Safety Journal*, **36 (**2001) pp745-767.

[11] Huang, Z., Burgess, I.W. and Plank, R.J., "Effective stiffness modelling of composite concrete slabs in fire", *Engineering Structures*, **22 (**2000) pp1133-1144.

[12] Lim, L.C.S., "*Membrane action in fire exposed concrete floor systems",* PhD thesis, University of Canterbury, New Zealand, 2003.

[13] Lim, L.C.S., Buchanan, A., Moss, P. and Franssen, J.-M., "Numerical modelling of two-way reinforced concrete slabs in fire", *Engineering Structures*, **26** (2004) pp1081-1091.

[14] Huang, Z., Burgess, I.W. and Plank, R.J., "3D modelling of beam-columns with general cross-sections in fire", Paper S6-5, Third International Workshop on Structures in Fire, Ottawa, Canada, 2004, pp323-334

[15] Lim, L.C.S. and Wade, C., "*Experimental fire tests of two-way concrete slabs"*, Fire Engineering Research Report 02/12, University of Canterbury, New Zealand, September 2002.

[16] Lennon, T., "*Results and observations from full-scale fire test at BRE Cardington, 16 January 2003"*, BRE client report 215-741, 2004.

[17] Wald, F., Chladná, M., Moore, D., Santiago, A., and Lennon, T., "The temperature distribution in a full-scale steel framed building subject to a natural fire", *Steel and Composite Structures*, **6** (2) (2006).

[18] Foster, S., Chladná, M., Hsieh, C., Burgess, I., and Plank, R., "Thermal and structural behaviour of a full-scale composite building subject to a severe compartment fire", *Fire Safety Journal, (In press)*.

[19] Wickström, U. and Sterner, E., *"TASEF-temperature analysis of structures exposed to fire-User's manual"*, Swedish National Testing Institute, SP Report 05, 1990.

TABLES

Table 1: Orthotropic slab deckings used in the parametric study (cases studied marked ✓).

Group	Decking wavelength L (mm)	L_0 (mm)	H_s (mm)	Rib Width Ratio (RWR)	α(°)					
					45	60	75	90	105	120
1	200	40	60	0.2			✓	✓		
2	200	60	40	0.3	✓	✓	✓	✓		
3	250	80	80	0.32		✓	✓	✓		
4	200	120	40	0.6	✓	✓	✓	✓	✓	✓
5	200	120	60	0.6	✓	✓	✓	✓	✓	✓
6	250	175	60	0.7	✓	✓	✓	✓	✓	✓
7	300	210	40	0.7	✓	✓	✓	✓	✓	✓

Table 2: A simple method to evaluate the structural performance of orthotropic slabs (fire resistance level increases with the summation of RWR and RDF).

Group	(1) Rib Width Ratio (RWR)	(2) Rib Depth Factor (RDF) = Depth of rib (mm) ÷ 100(mm)	(1) + (2)	Fire resistance level
1	0.20	0.60	0.80	C
2	0.30	0.40	0.70	C
3	0.32	0.80	1.12	B
4	0.60	0.40	1.00	B
5	0.60	0.60	1.20	A
6	0.70	0.60	1.30	A
7	0.70	0.40	1.10	B

FIGURE CAPTIONS

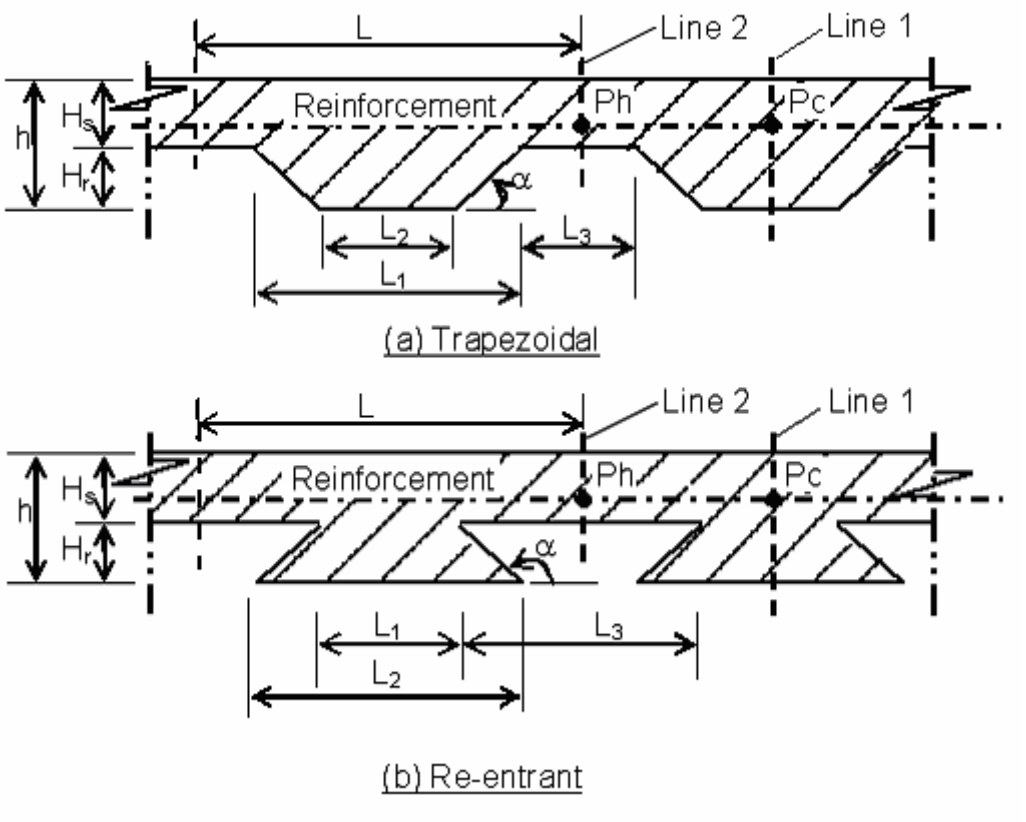
L
Line 2
Line 1
Reinforcement
Ph
Pc
h
Hs
Hr
α
L2
L3
L1
(a) Trapezoidal
L
Line 2
Line 1
Reinforcement
Ph
Pc
h
Hs
Hr
α
L1
L3
L2
(b) Re-entrant

Fig. 1

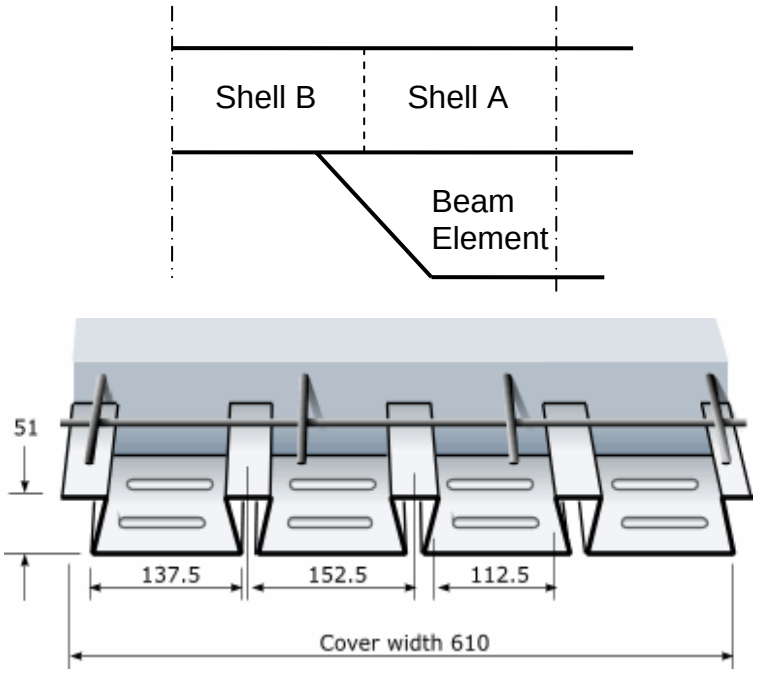

(a) Lim *et al.*'s model

(b) A typical decking for which Lim's model is unsuitable

Fig. 2

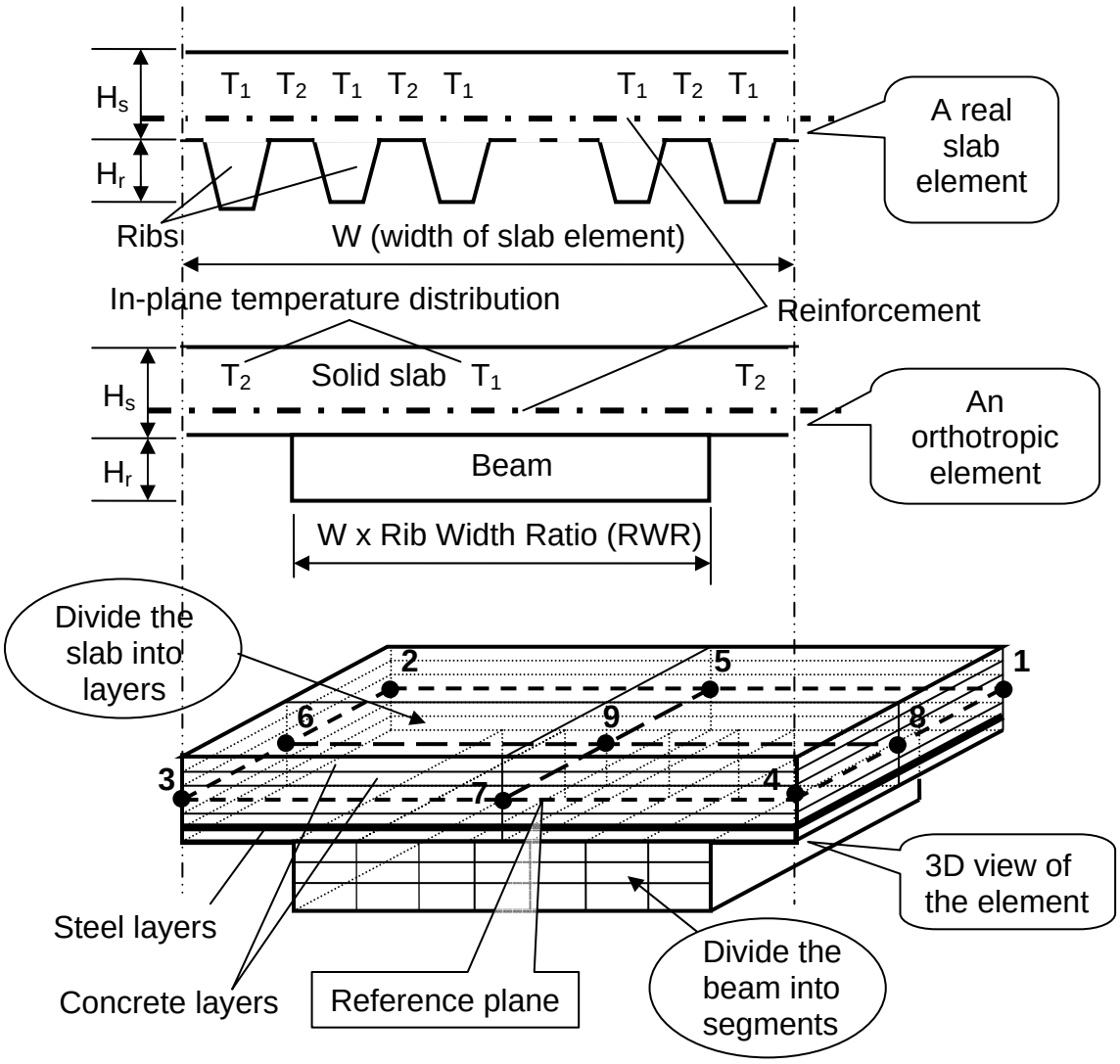
Hs
Hr
T1 T2 T1 T2 T1
T1 T2 T1
A real slab element
Ribs
W (width of slab element)
In-plane temperature distribution
Reinforcement
T2
Solid slab
T1
T2
Hs
Hr
An orthotropic element
Beam
W x Rib Width Ratio (RWR)
Divide the slab into layers
1
2
3
4
5
6
7
8
9
3D view of the element
Steel layers
Concrete layers
Reference plane
Divide the beam into segments

Fig. 3

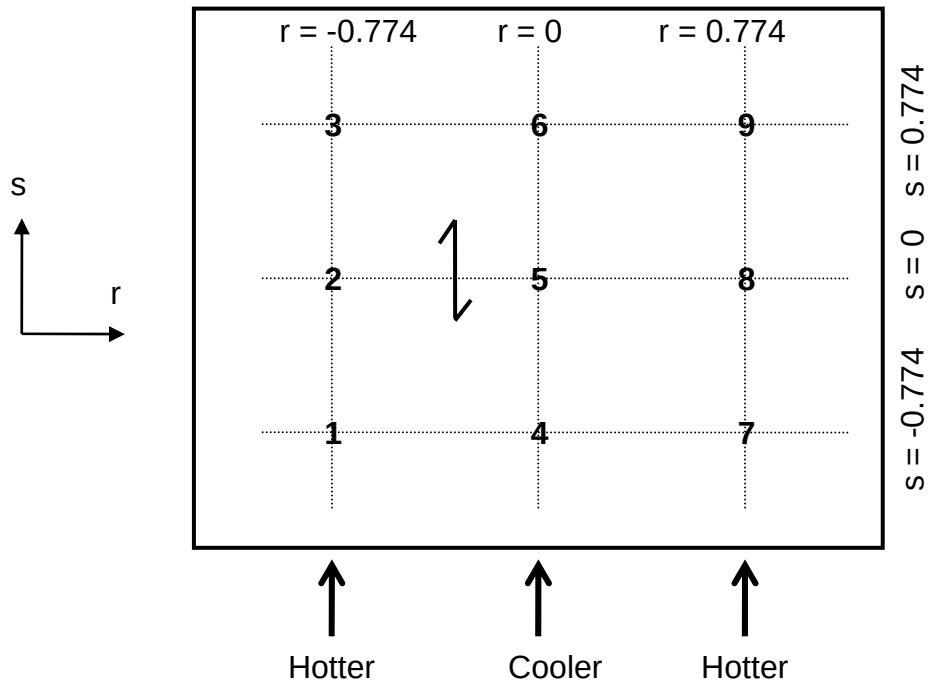
r = -0.774
r = 0
r = 0.774
3
6
9
2
5
8
1
4
7
s
r
s = 0.774
s = 0
s = -0.774
Hotter
Cooler
Hotter

Fig. 4

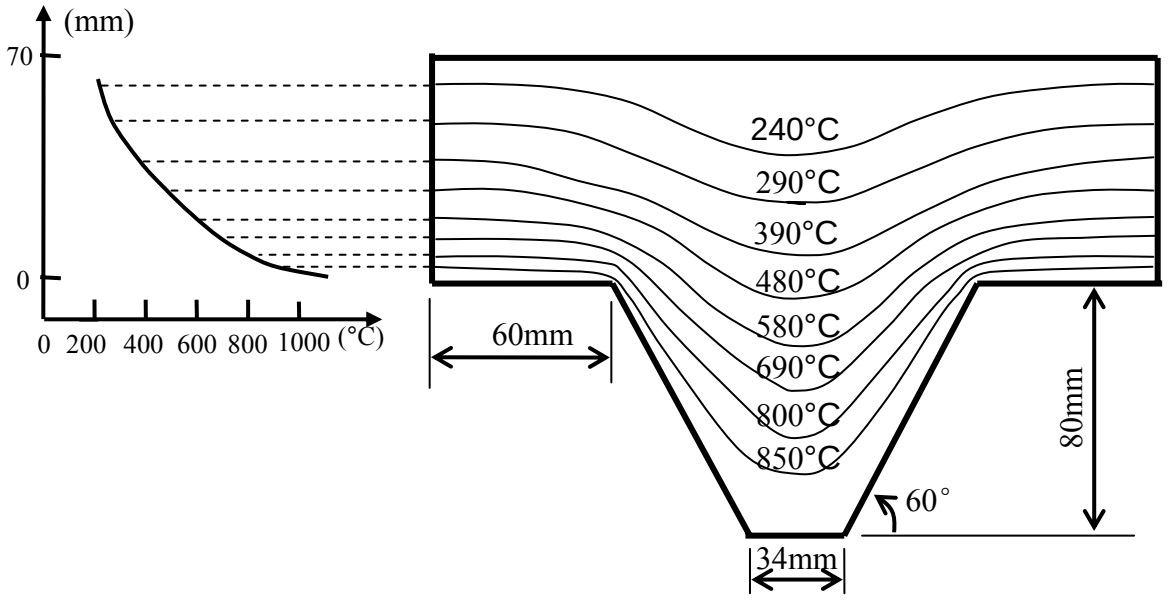
(mm)
70
0
0 200 400 600 800 1000 (°C)
240°C
290°C
390°C
480°C
580°C
690°C
800°C
850°C
60mm
80mm
60°
34mm

Fig. 5

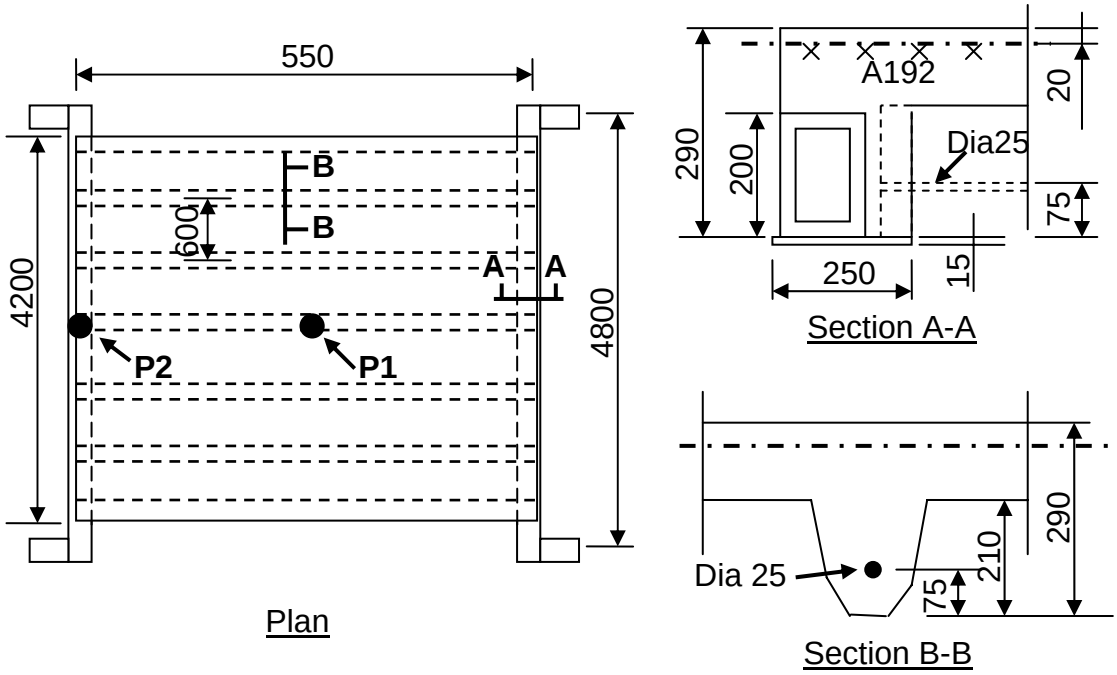

All dimensions in mm

Fig. 6

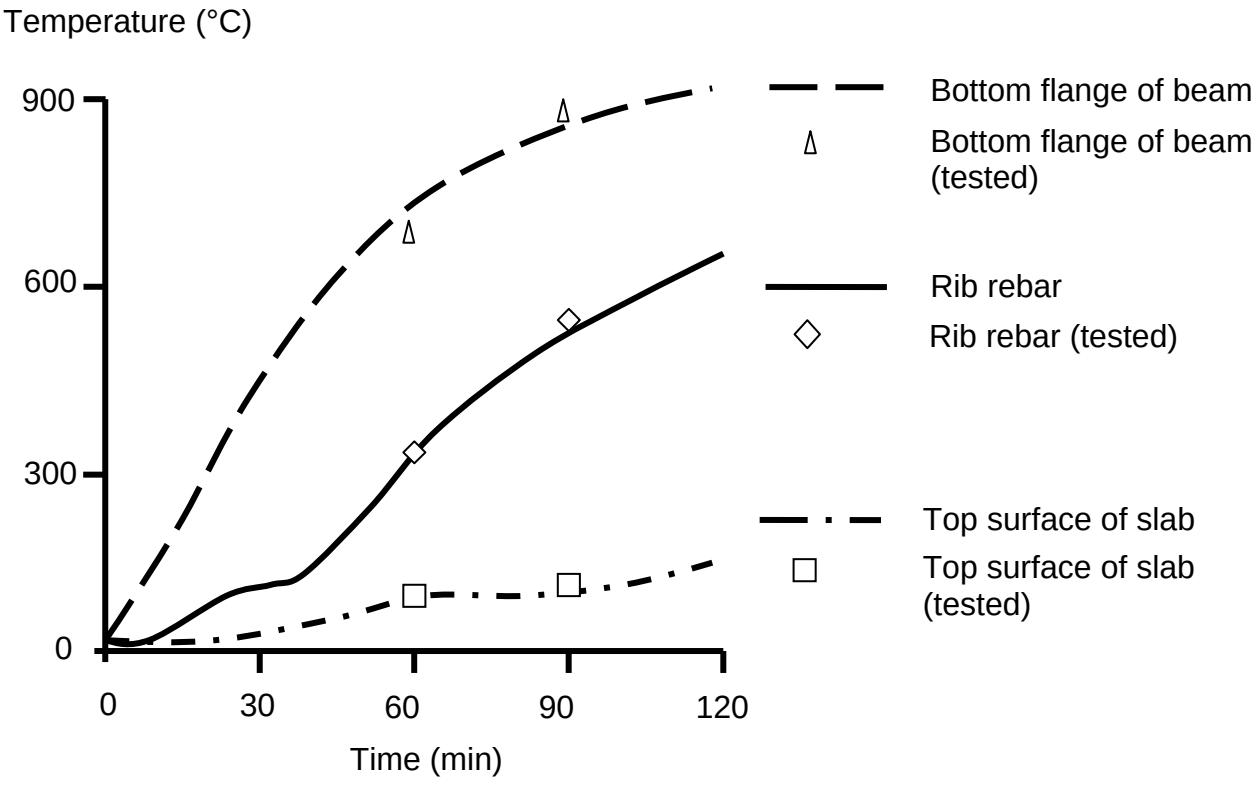
Temperature (°C)
900
600
300
0
0
30
60
90
120
Time (min)
Bottom flange of beam
Bottom flange of beam (tested)
Rib rebar
Rib rebar (tested)
Top surface of slab
Top surface of slab (tested)

Fig. 7

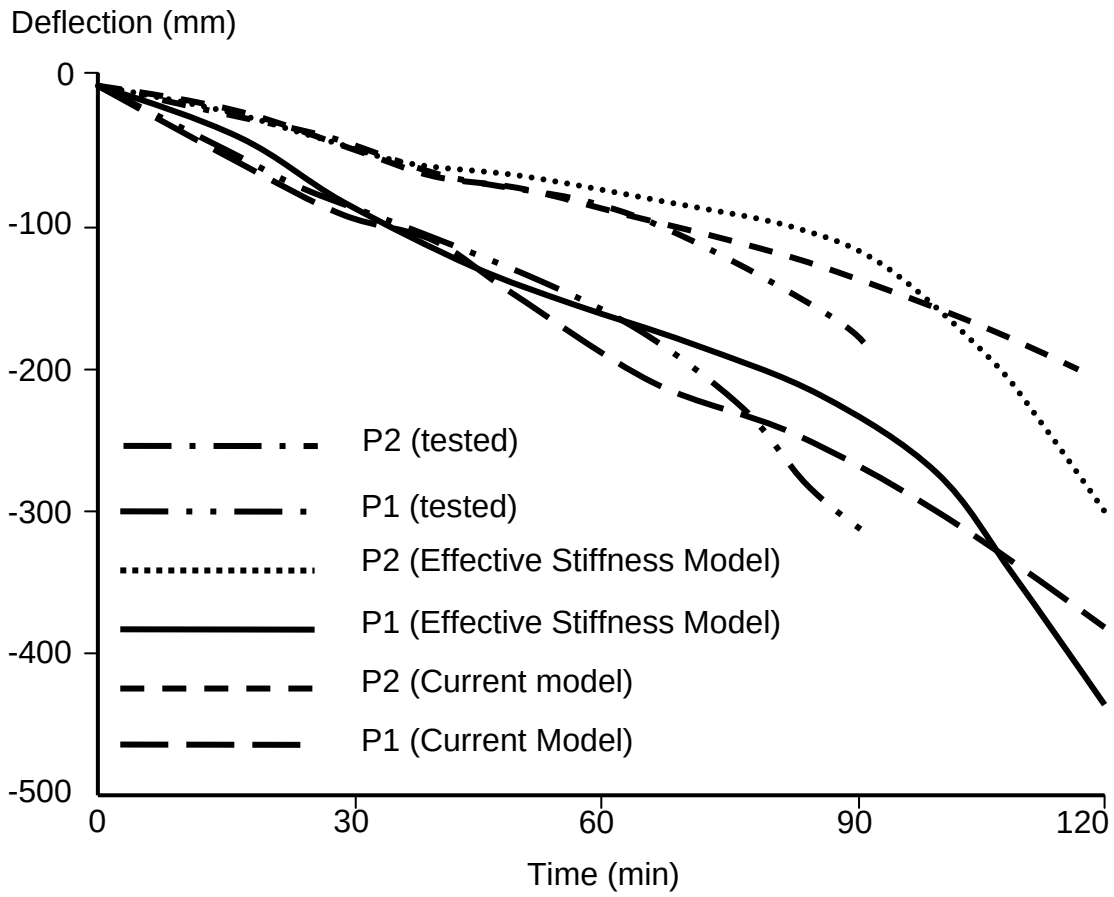
Deflection (mm)
0
-100
-200
-300
-400
-500
0
30
60
90
120
Time (min)
P2 (tested)
P1 (tested)
P2 (Effective Stiffness Model)
P1 (Effective Stiffness Model)
P2 (Current model)
P1 (Current Model)

Fig. 8

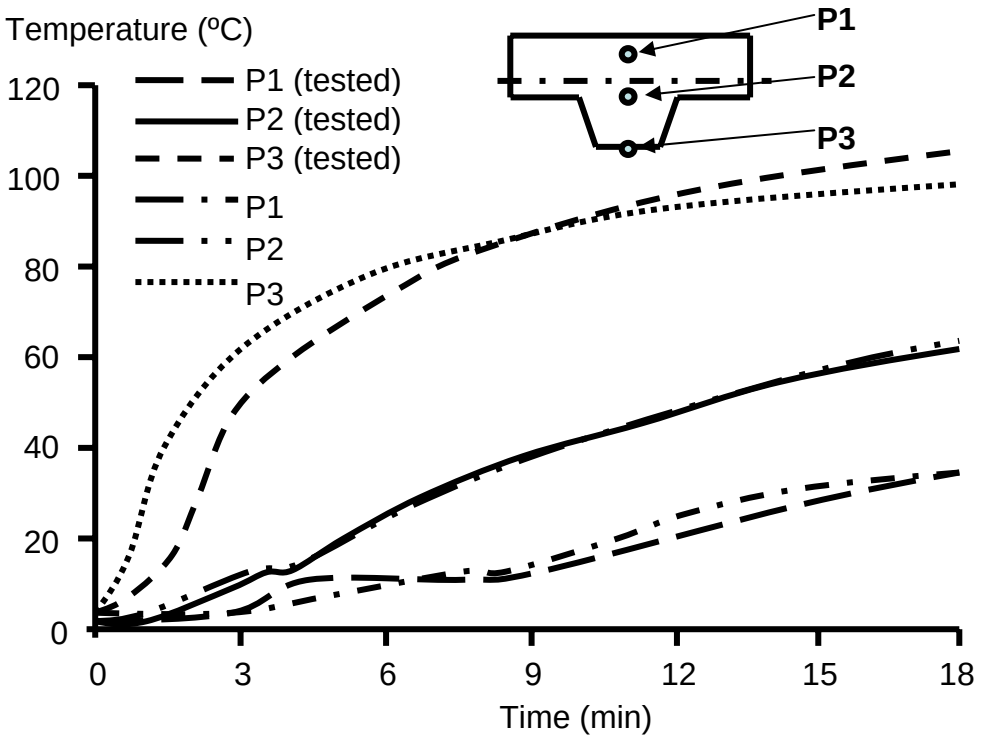
Temperature (ºC)
P1 (tested)
P2 (tested)
P3 (tested)
P1
P2
P3
P1
P2
P3
120
100
80
60
40
20
0
0
3
6
9
12
15
18
Time (min)

Fig. 9

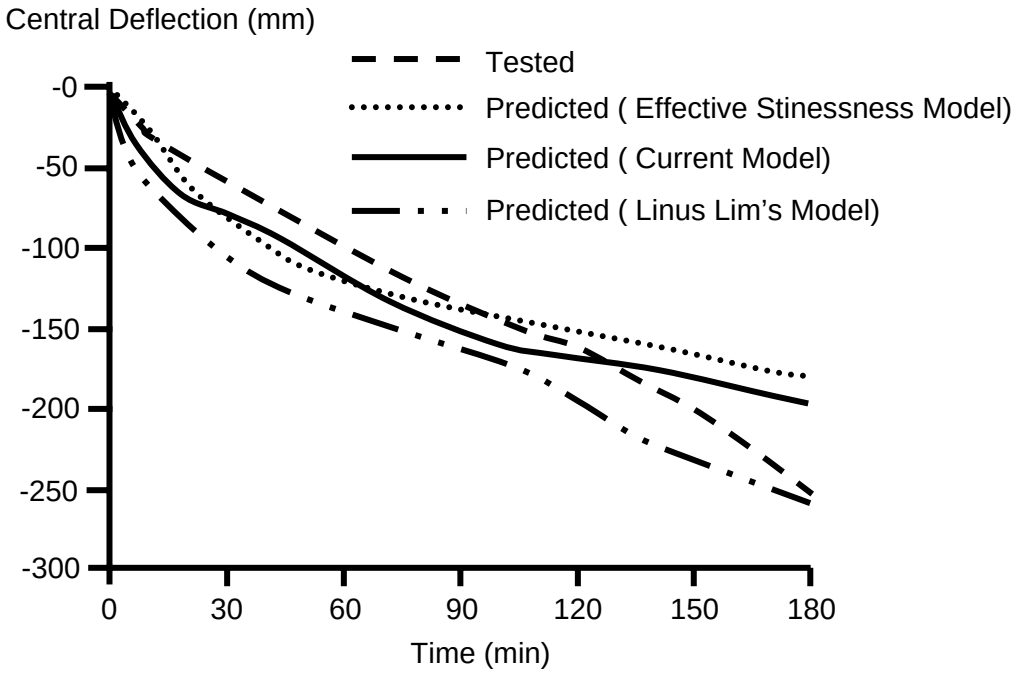
Central Deflection (mm)
Tested
Predicted (Effective Stinessness Model)
Predicted (Current Model)
Predicted (Linus Lim's Model)
-0
-50
-100
-150
-200
-250
-300
0
30
60
90
120
150
180
Time (min)

Fig. 10

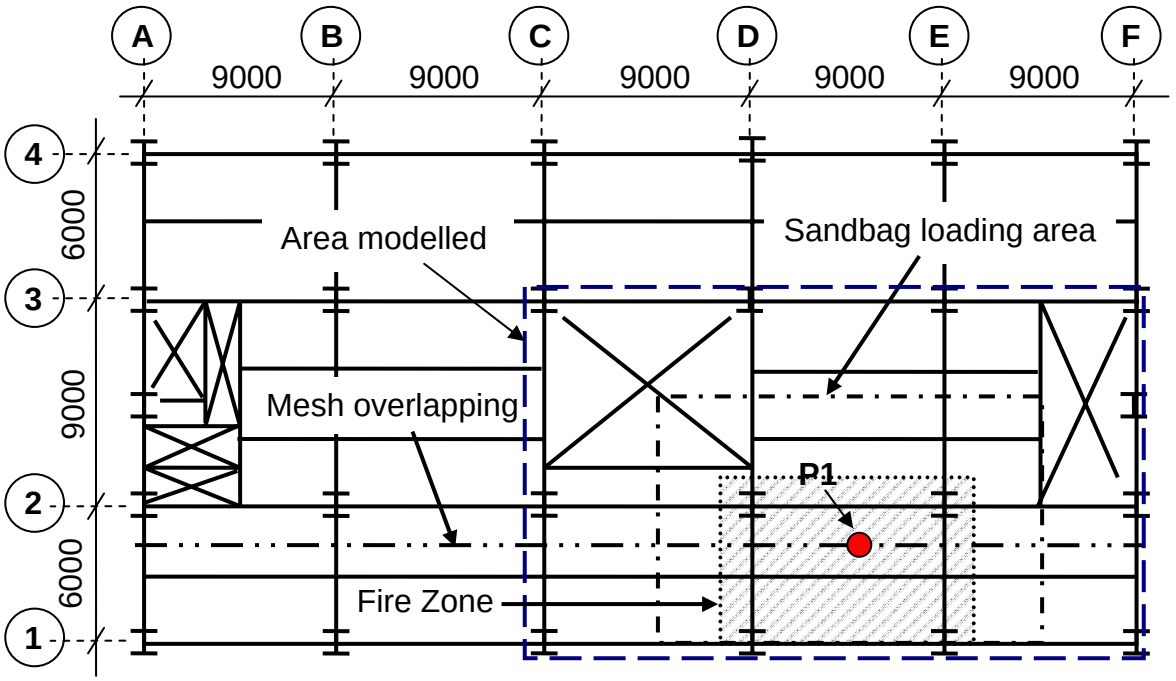

All dimensions in mm

Fig. 11

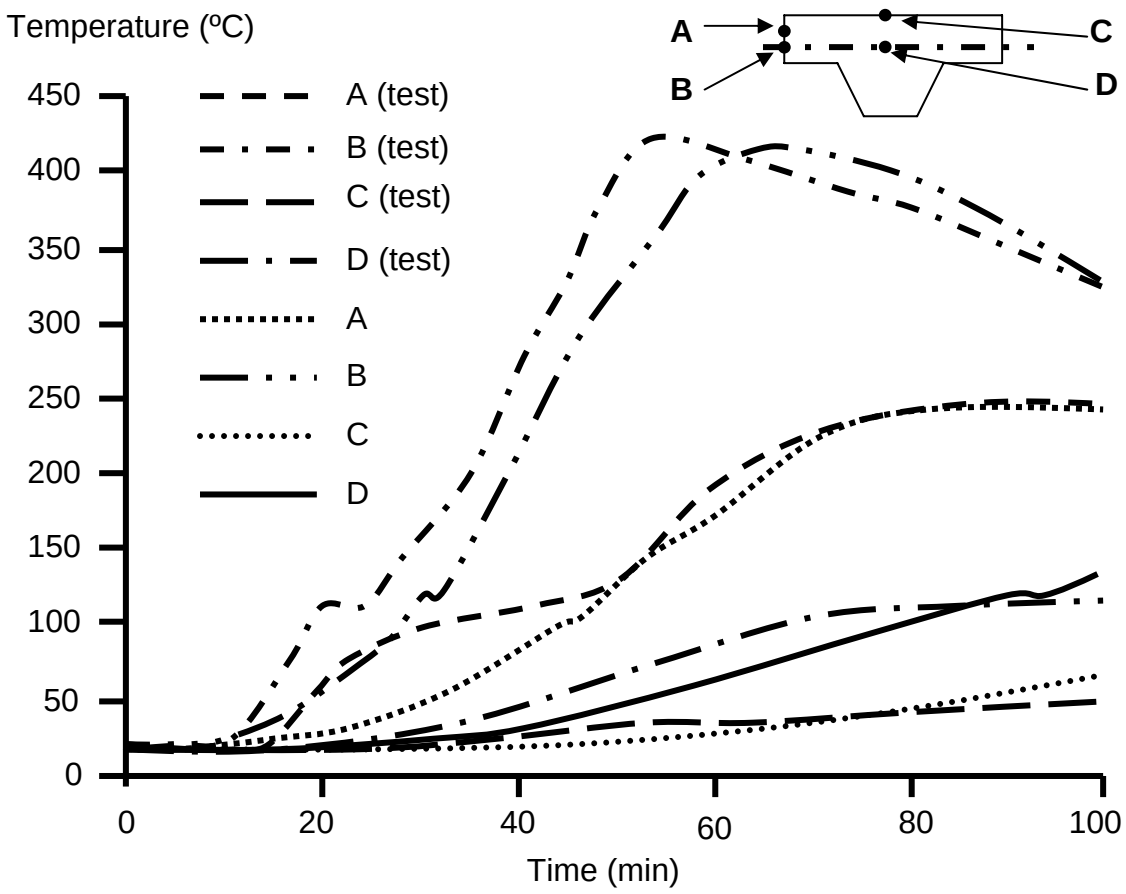
Temperature (ºC)
450
400
350
300
250
200
150
100
50
0
A (test)
B (test)
C (test)
D (test)
A
B
C
D
0
20
40
60
80
100
Time (min)
A
B
C
D

Fig. 12

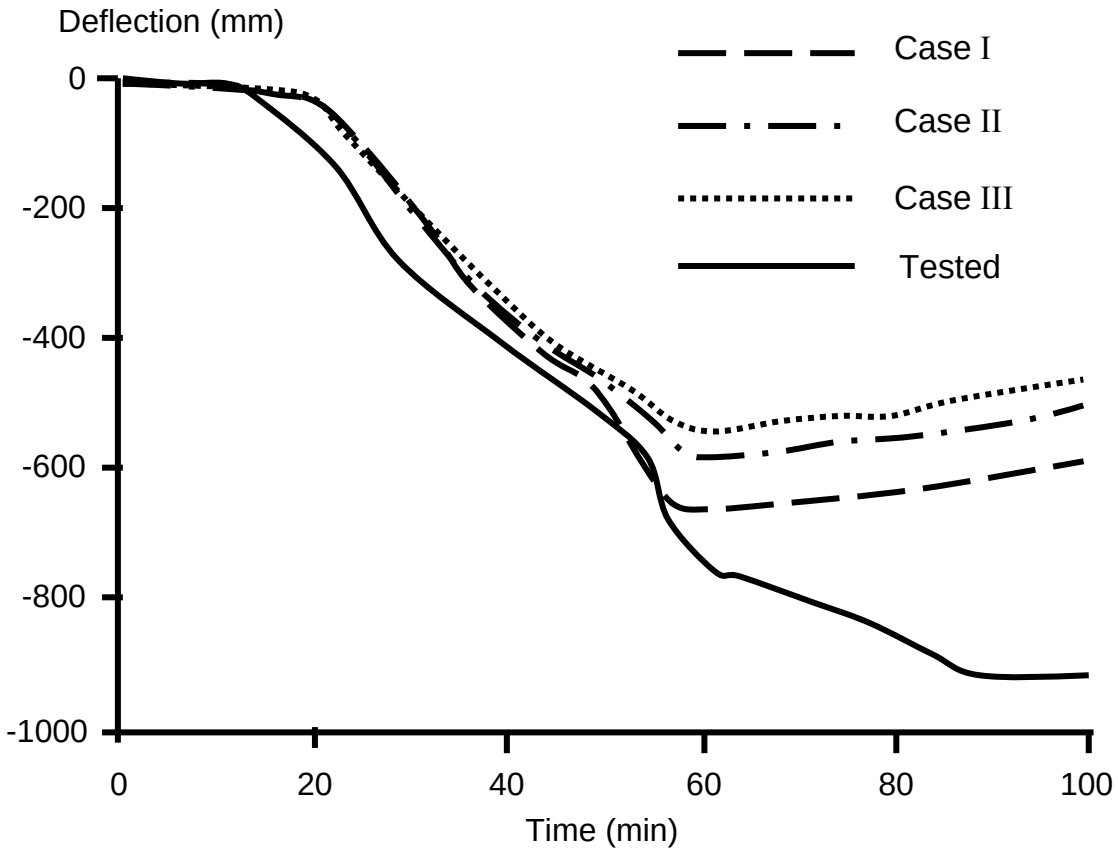
Deflection (mm)
0
-200
-400
-600
-800
-1000
0
20
40
60
80
100
Time (min)
Case I
Case II
Case III
Tested

Fig. 13

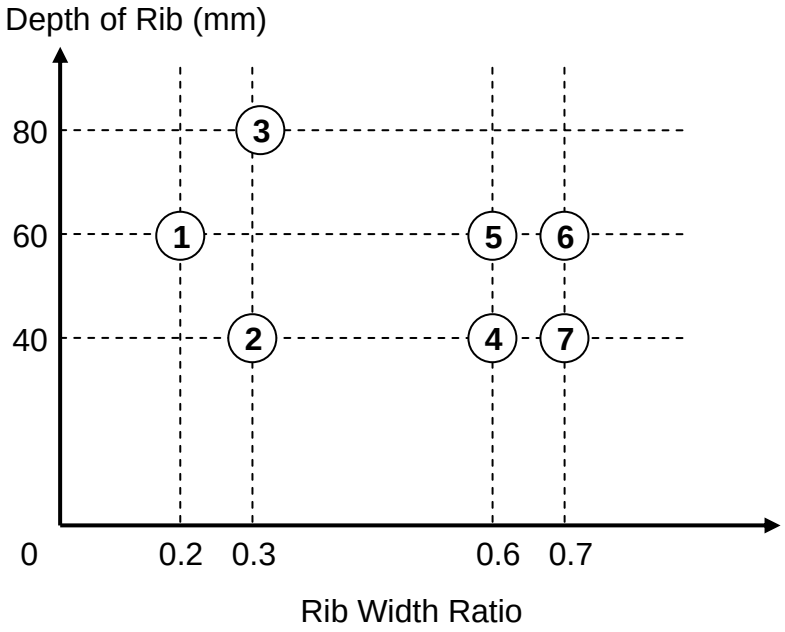
Depth of Rib (mm)
80
60
40
0
0.2
0.3
0.6
0.7
Rib Width Ratio
1
2
3
4
5
6
7

Fig. 14

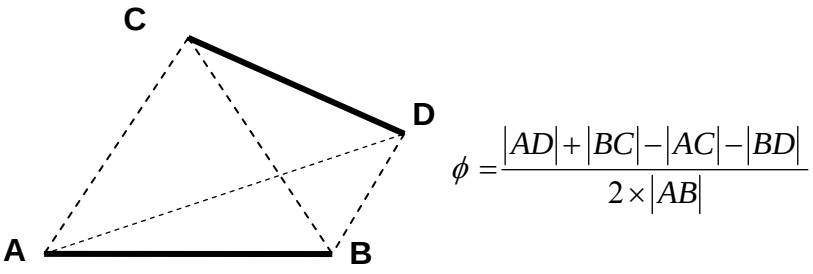
C
D
A
B
$\phi = \frac{|AD| + |BC| - |AC| - |BD|}{2 \times |AB|}$

Fig. 15

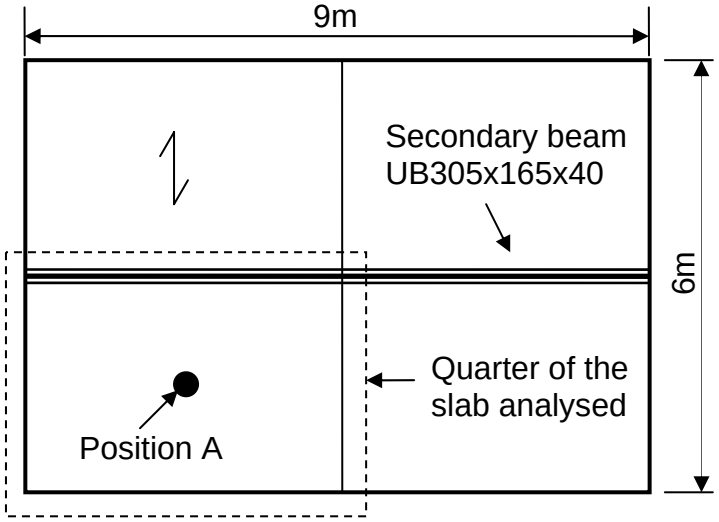
9m
Secondary beam
UB305x165x40
6m
Quarter of the
slab analysed
Position A

Fig. 16

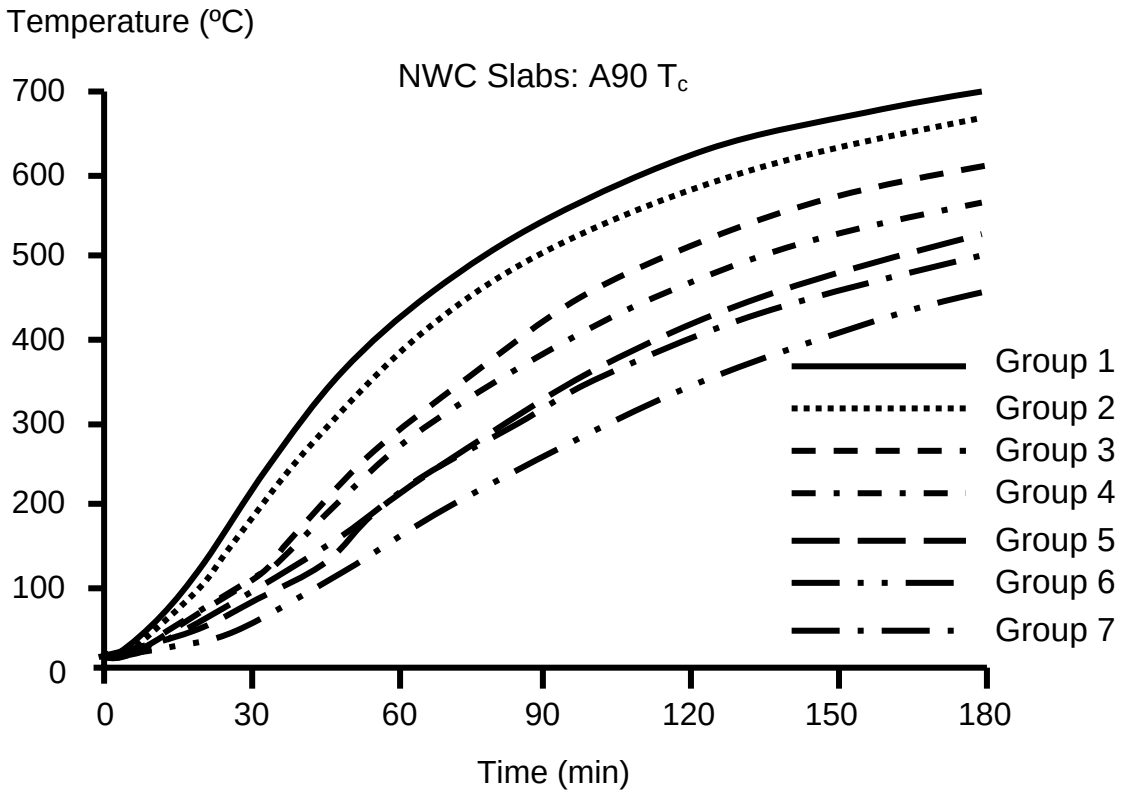
Temperature (ºC)
NWC Slabs: A90 T_c
700
600
500
400
300
200
100
0
0
30
60
90
120
150
180
Time (min)
Group 1
Group 2
Group 3
Group 4
Group 5
Group 6
Group 7

Fig. 17 (a)

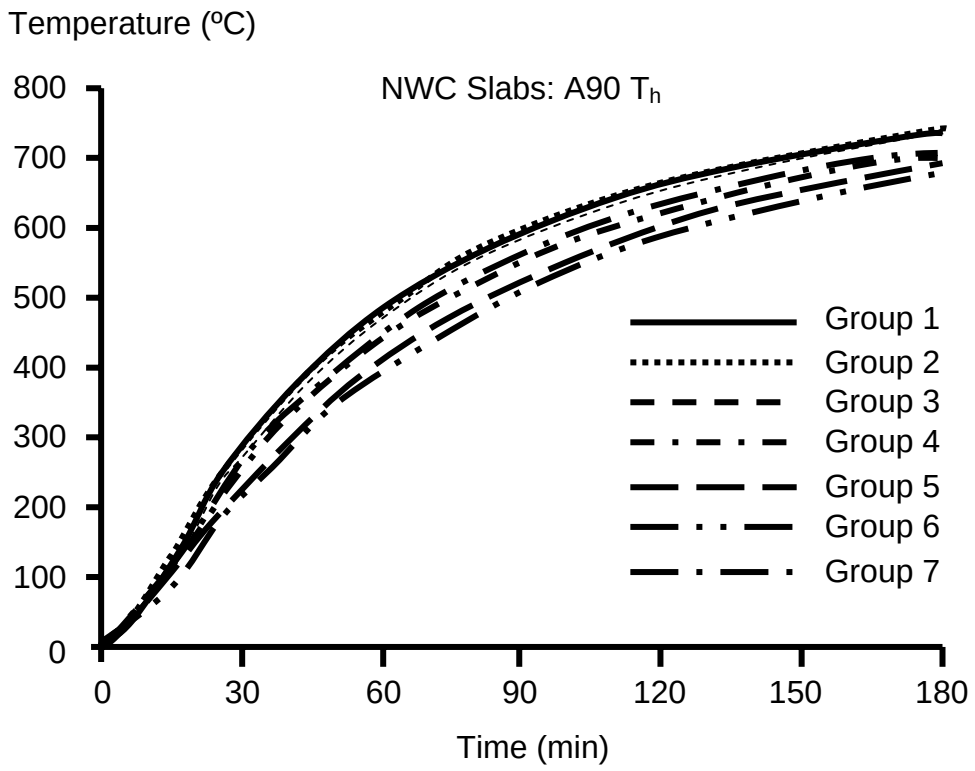
Temperature (ºC)
NWC Slabs: A90 T_h
800
700
600
500
400
300
200
100
0
0
30
60
90
120
150
180
Time (min)
Group 1
Group 2
Group 3
Group 4
Group 5
Group 6
Group 7

Fig. 17 (b)

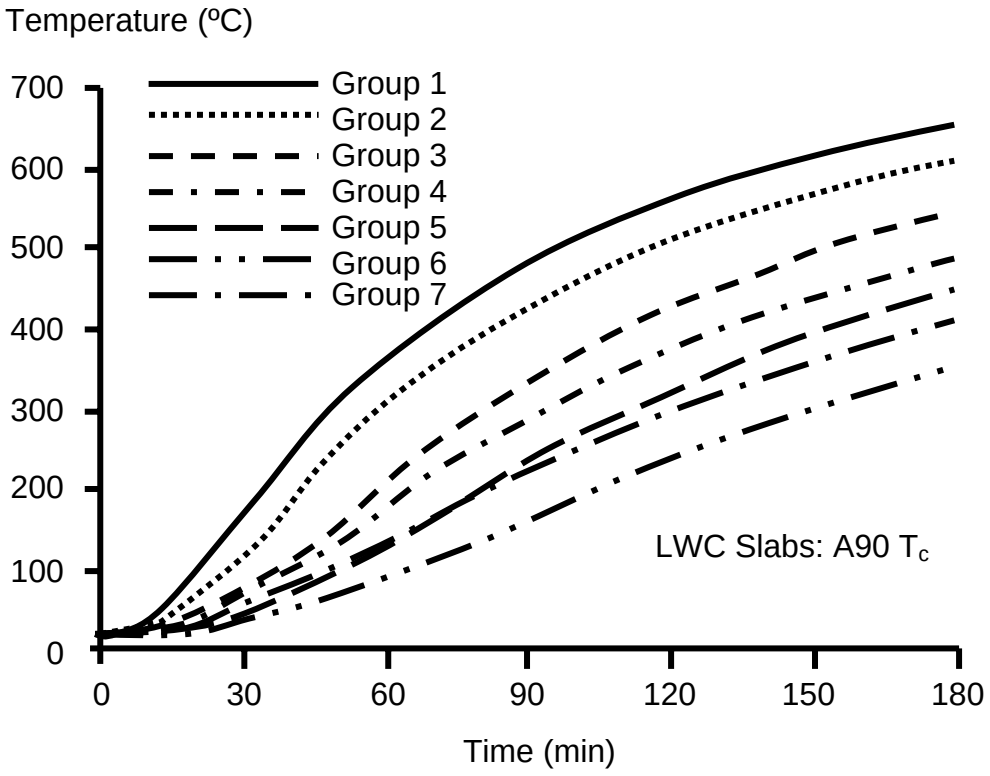
Temperature (ºC)
700
600
500
400
300
200
100
0
Group 1
Group 2
Group 3
Group 4
Group 5
Group 6
Group 7
LWC Slabs: A90 T_c
0
30
60
90
120
150
180
Time (min)

Fig. 18 (a)

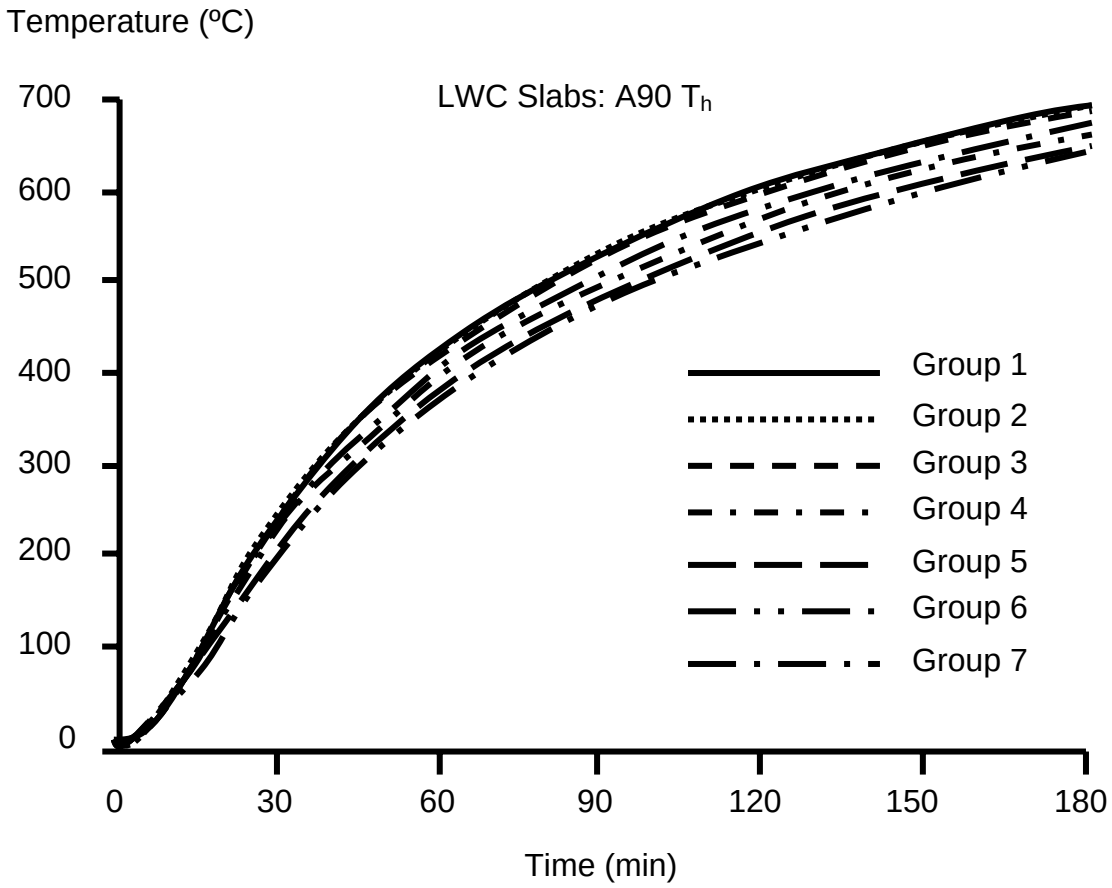
Temperature (ºC)
LWC Slabs: A90 T_h
700
600
500
400
300
200
100
0
0
30
60
90
120
150
180
Time (min)
Group 1
Group 2
Group 3
Group 4
Group 5
Group 6
Group 7

Fig. 18 (b)

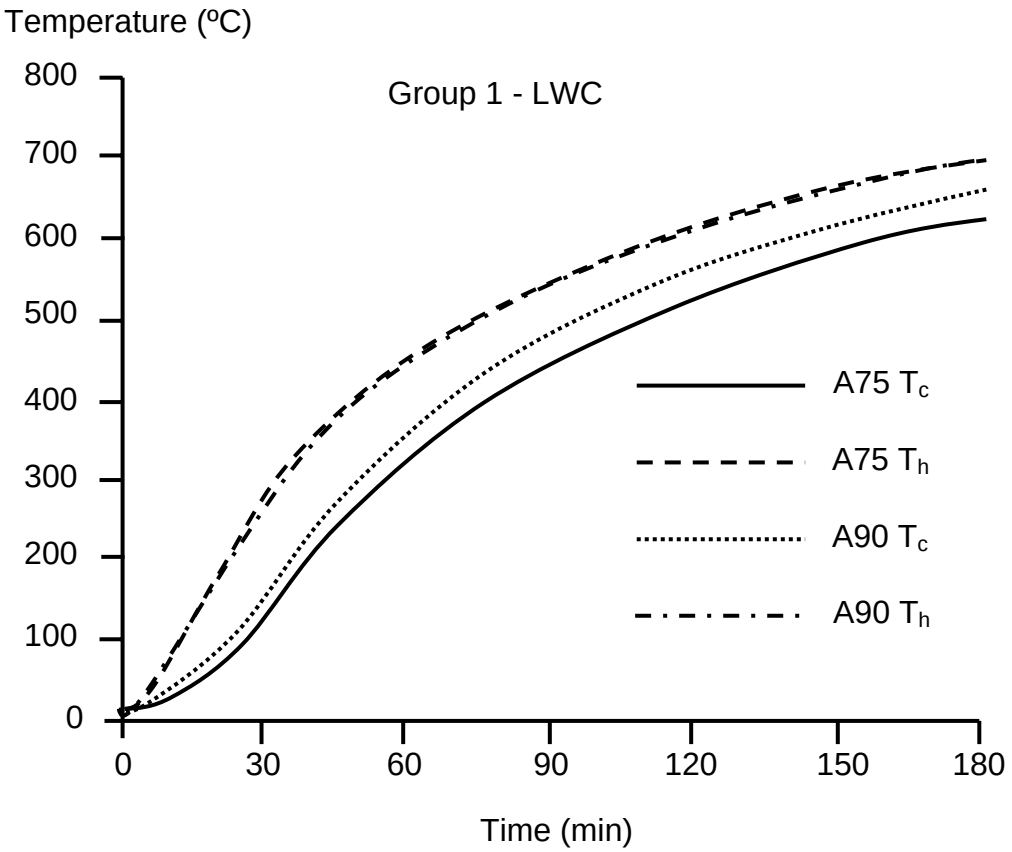
Temperature (ºC)
Group 1 - LWC
800
700
600
500
400
300
200
100
0
0
30
60
90
120
150
180
Time (min)
A75 T_c
A75 T_h
A90 T_c
A90 T_h

Fig. 19 (a)

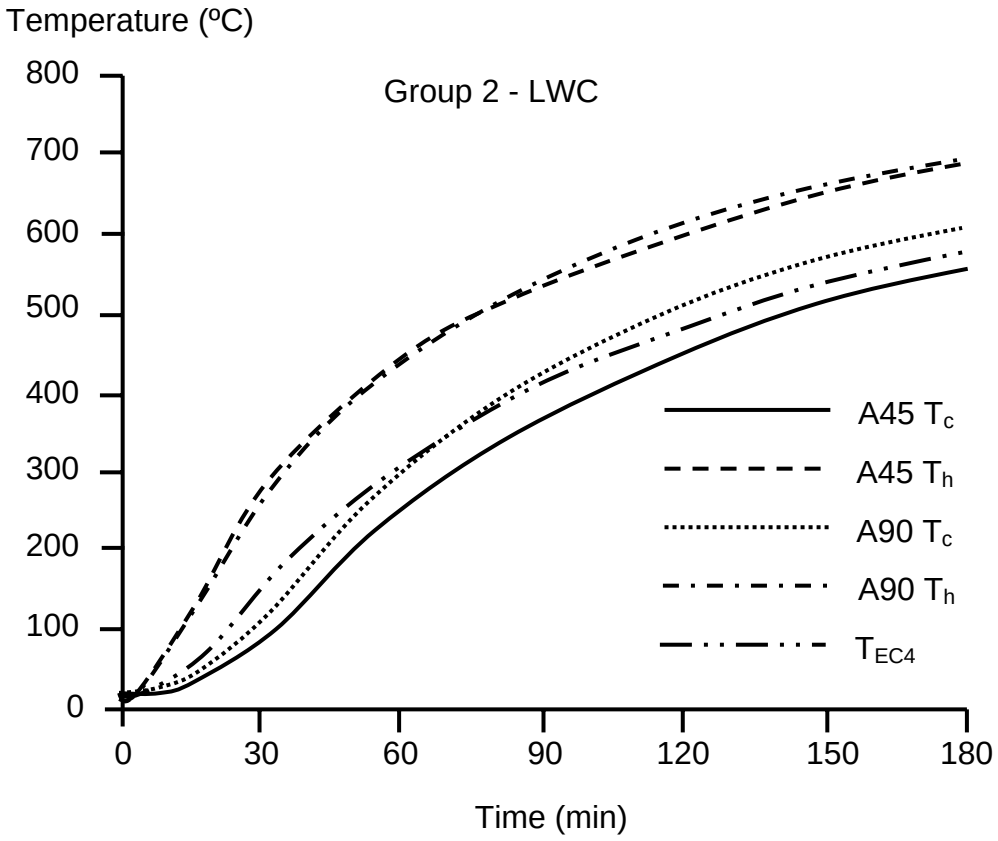
Temperature (ºC)
Group 2 - LWC
800
700
600
500
400
300
200
100
0
0
30
60
90
120
150
180
Time (min)
A45 T_c
A45 T_h
A90 T_c
A90 T_h
T_{EC4}

Fig. 19 (b)

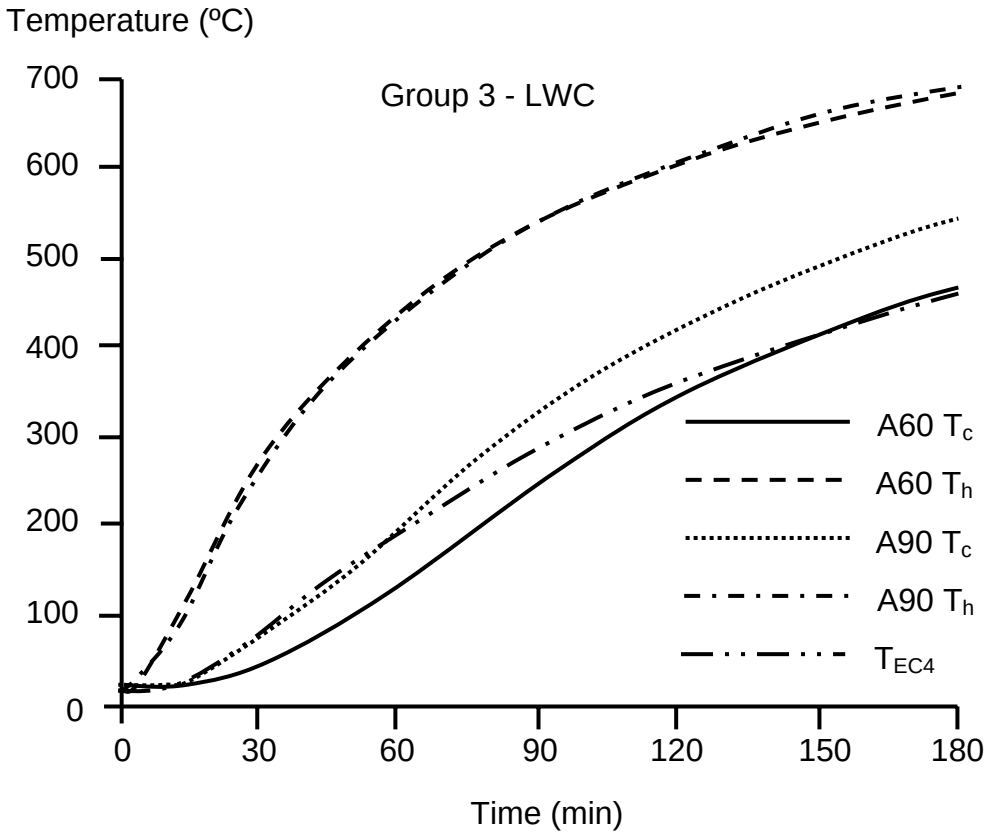
Temperature (ºC)
Group 3 - LWC
700
600
500
400
300
200
100
0
0
30
60
90
120
150
180
Time (min)
A60 T_c
A60 T_h
A90 T_c
A90 T_h
T_{EC4}

Fig. 19 (c)

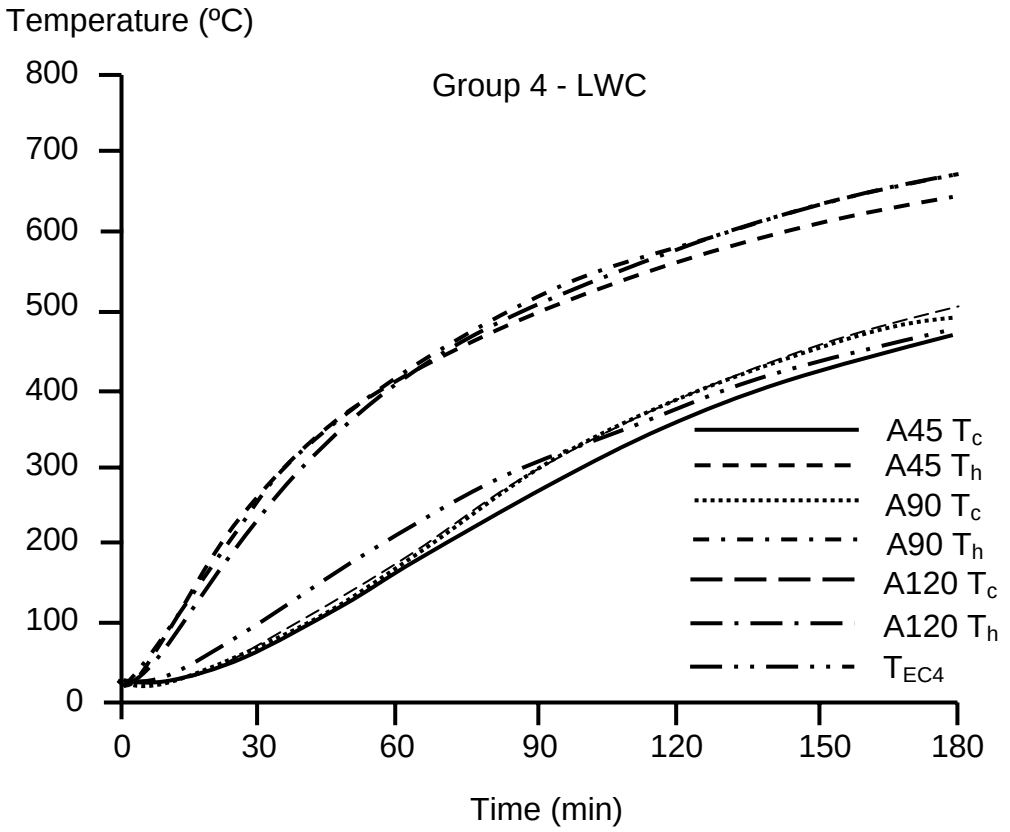
Temperature (ºC)
Group 4 - LWC
800
700
600
500
400
300
200
100
0
0
30
60
90
120
150
180
Time (min)
A45 T_c
A45 T_h
A90 T_c
A90 T_h
A120 T_c
A120 T_h
T_{EC4}

Fig. 19 (d)

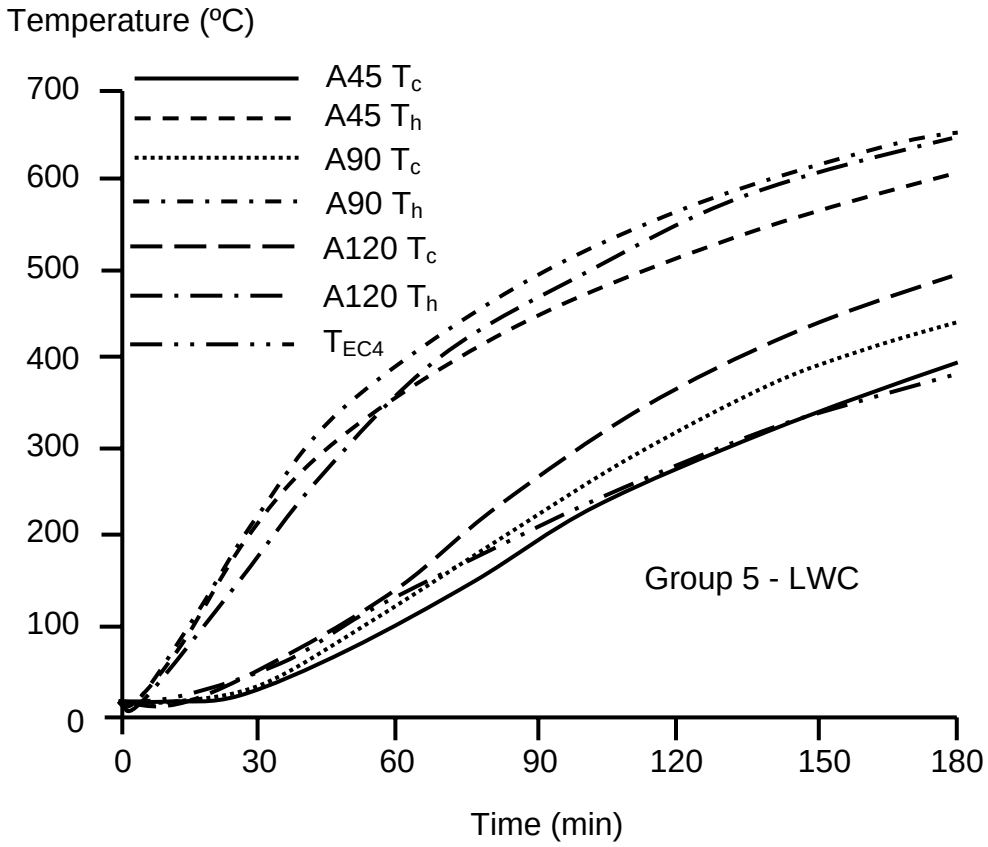
Temperature (ºC)
A45 T_c
A45 T_h
A90 T_c
A90 T_h
A120 T_c
A120 T_h
T_{EC4}
700
600
500
400
300
200
100
0
0
30
60
90
120
150
180
Time (min)
Group 5 - LWC

Fig. 19 (e)

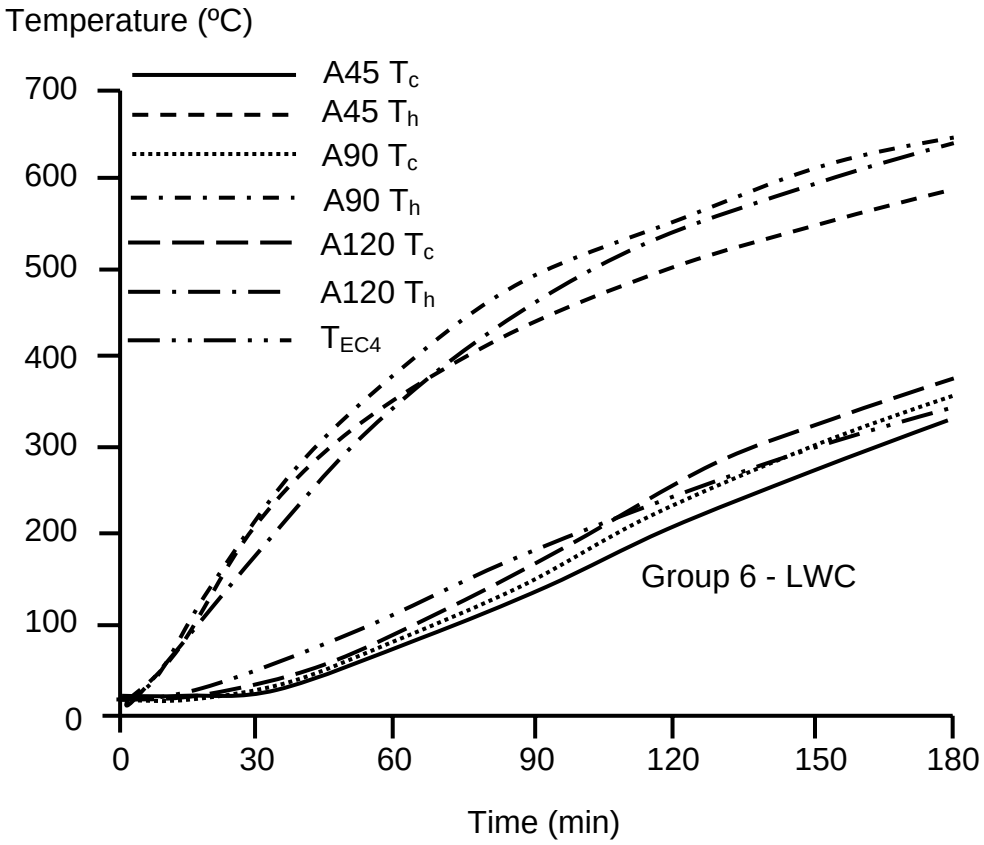
Temperature (ºC)
A45 T_c
A45 T_h
A90 T_c
A90 T_h
A120 T_c
A120 T_h
T_{EC4}
700
600
500
400
300
200
100
0
0
30
60
90
120
150
180
Time (min)
Group 6 - LWC

Fig. 19 (f)

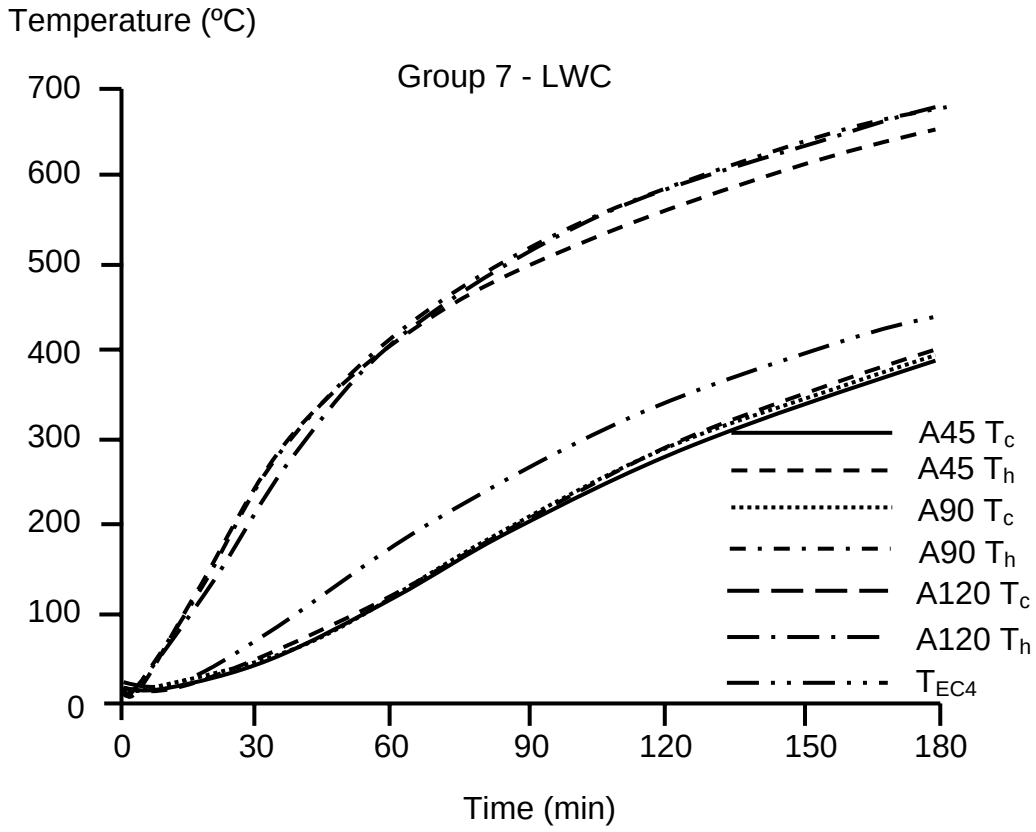
Temperature (ºC)
Group 7 - LWC
700
600
500
400
300
200
100
0
0
30
60
90
120
150
180
Time (min)
A45 T_c
A45 T_h
A90 T_c
A90 T_h
A120 T_c
A120 T_h
T_{EC4}

Fig. 19 (g)

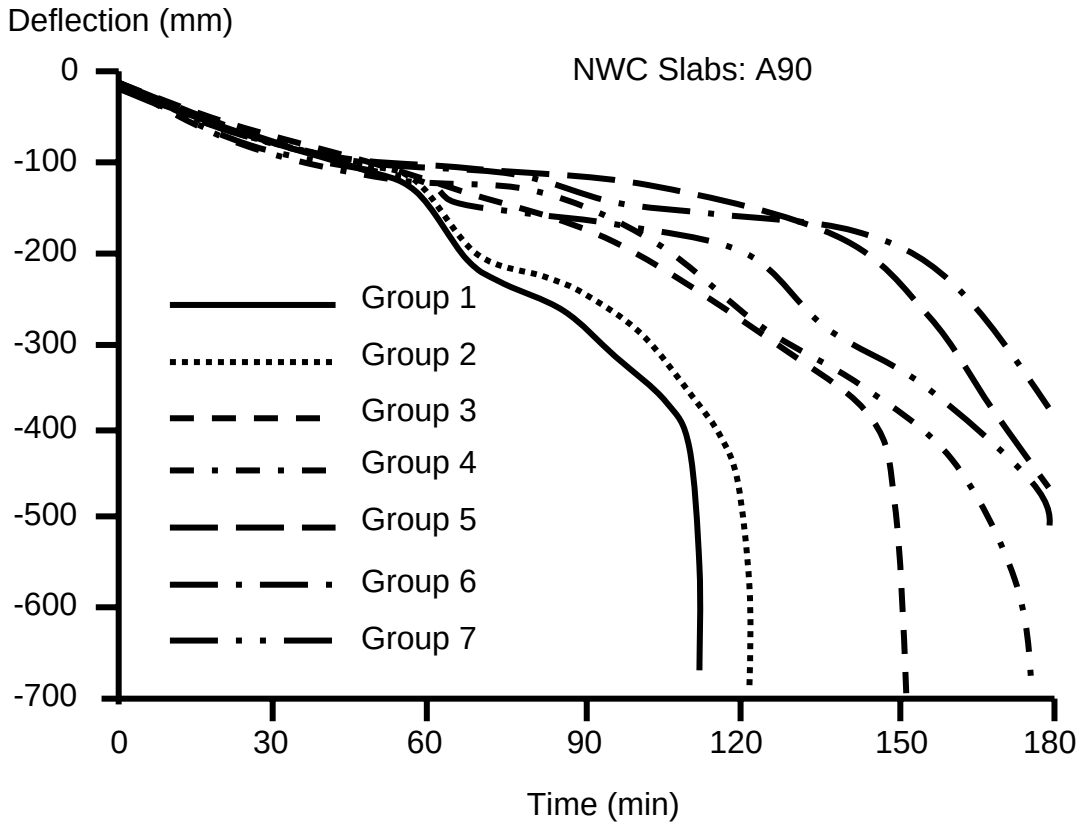
Deflection (mm)
NWC Slabs: A90
0
-100
-200
-300
-400
-500
-600
-700
Group 1
Group 2
Group 3
Group 4
Group 5
Group 6
Group 7
0
30
60
90
120
150
180
Time (min)

Fig. 20

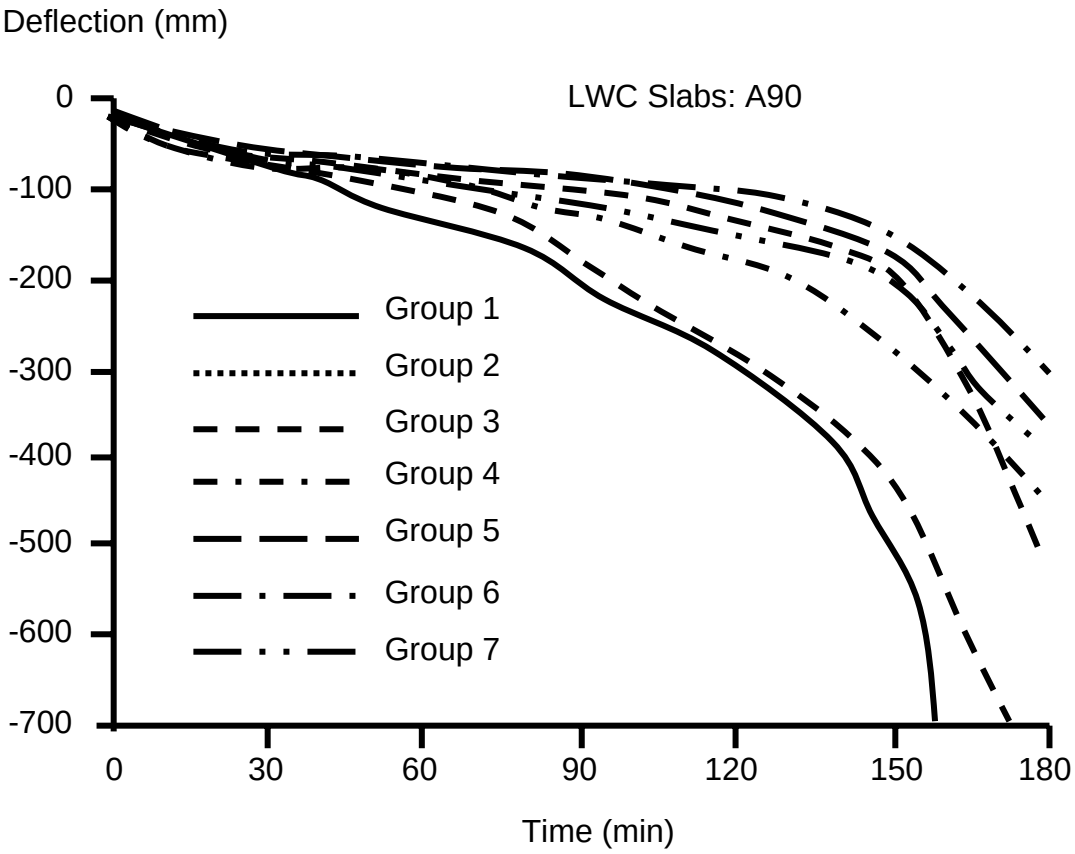
Deflection (mm)
LWC Slabs: A90
0
-100
-200
-300
-400
-500
-600
-700
0
30
60
90
120
150
180
Time (min)
Group 1
Group 2
Group 3
Group 4
Group 5
Group 6
Group 7

Fig. 21

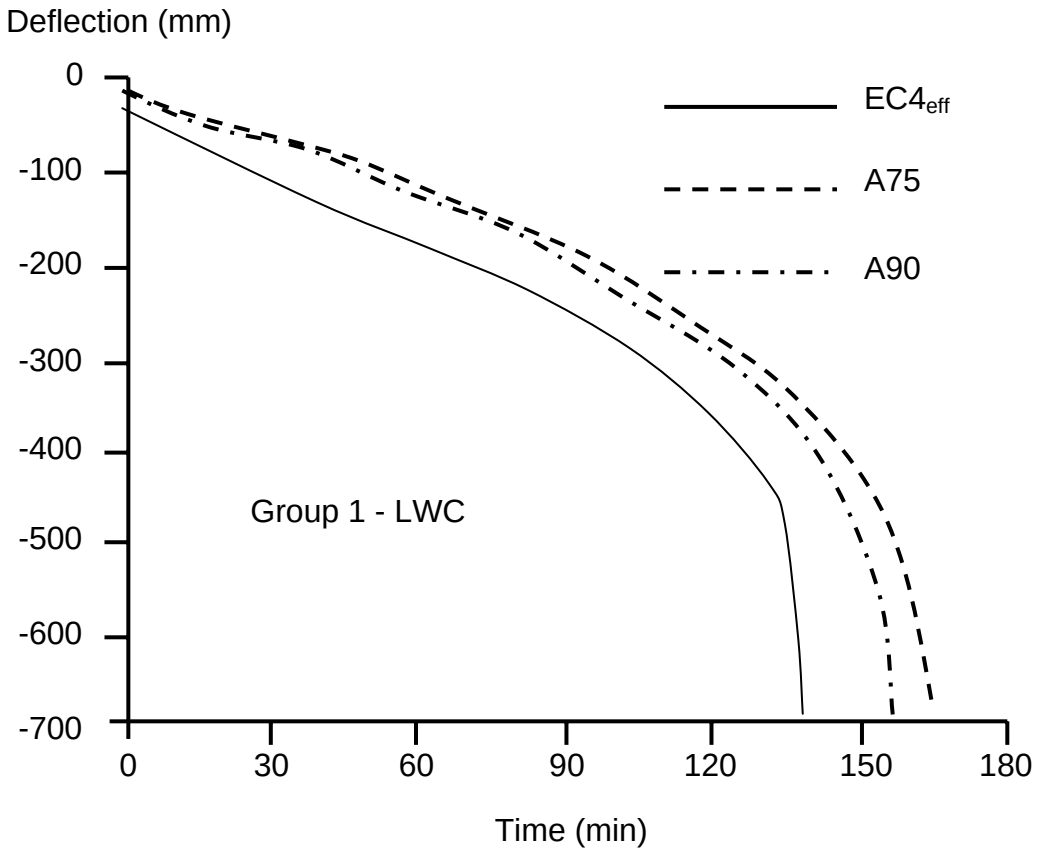
Deflection (mm)
0
-100
-200
-300
-400
-500
-600
-700
0
30
60
90
120
150
180
Time (min)
EC4eff
A75
A90
Group 1 - LWC

Fig. 22 (a)

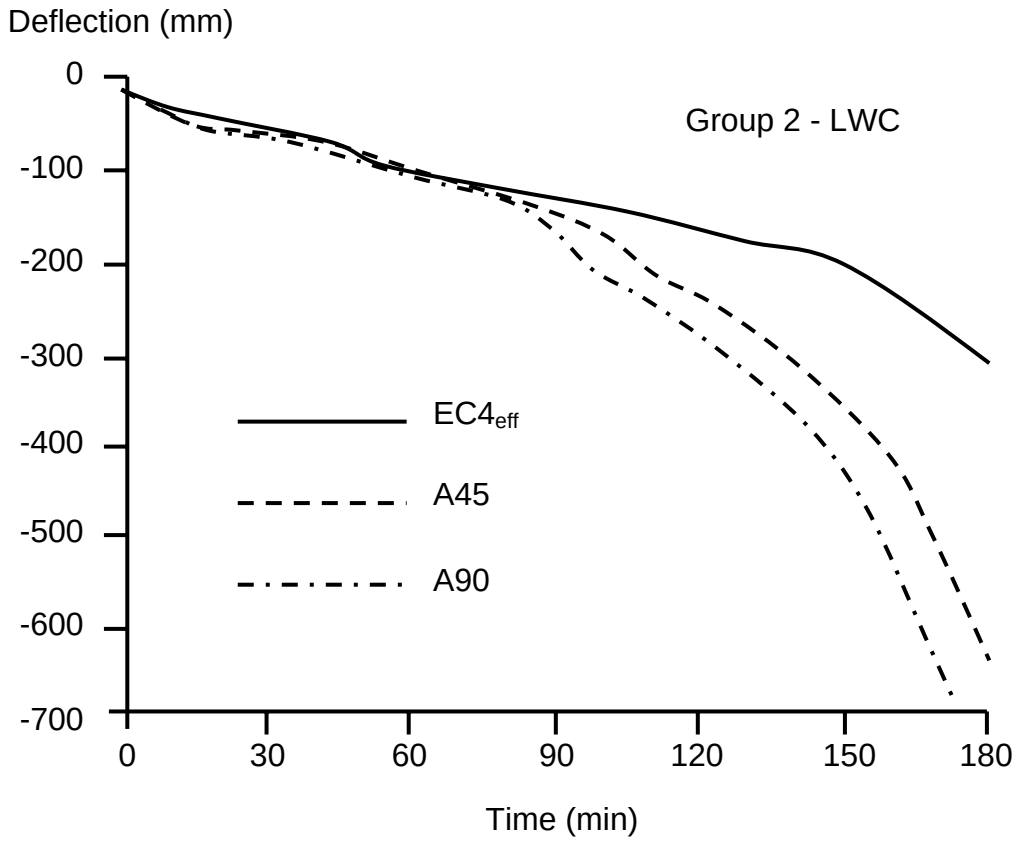
Deflection (mm)
0
-100
-200
-300
-400
-500
-600
-700
Group 2 - LWC
EC4eff
A45
A90
0
30
60
90
120
150
180
Time (min)

Fig. 22 (b)

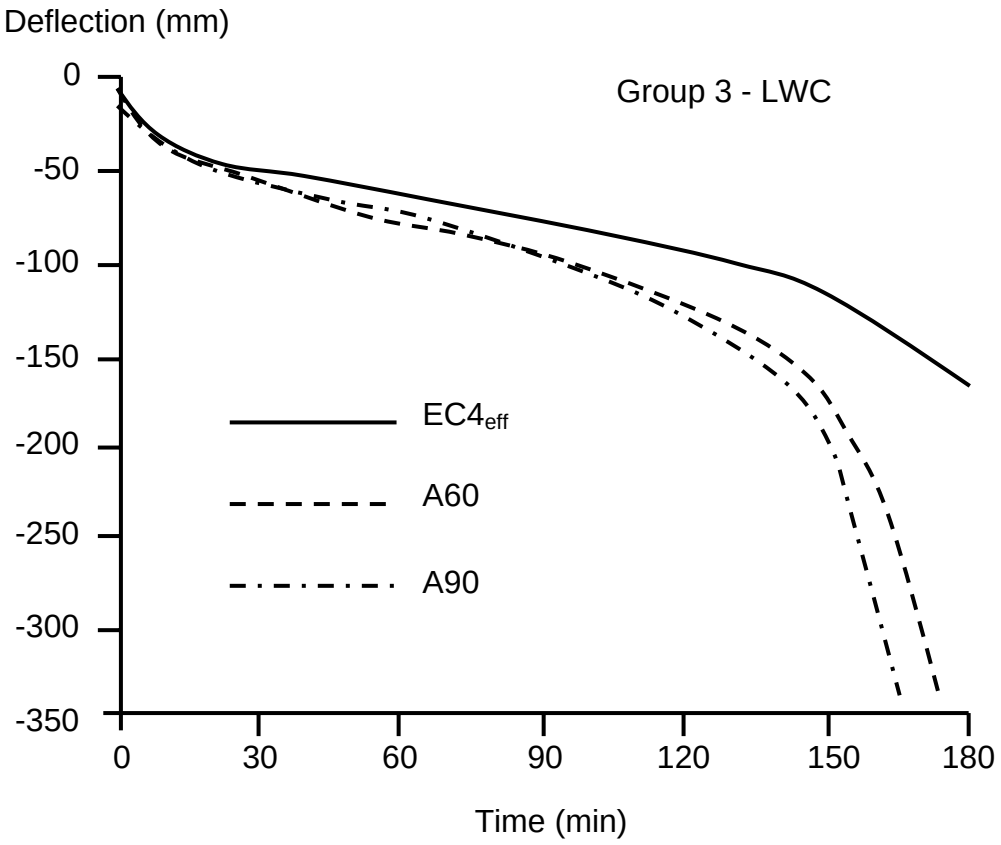
Deflection (mm)
0
-50
-100
-150
-200
-250
-300
-350
Group 3 - LWC
EC4eff
A60
A90
0
30
60
90
120
150
180
Time (min)

Fig. 22 (c)

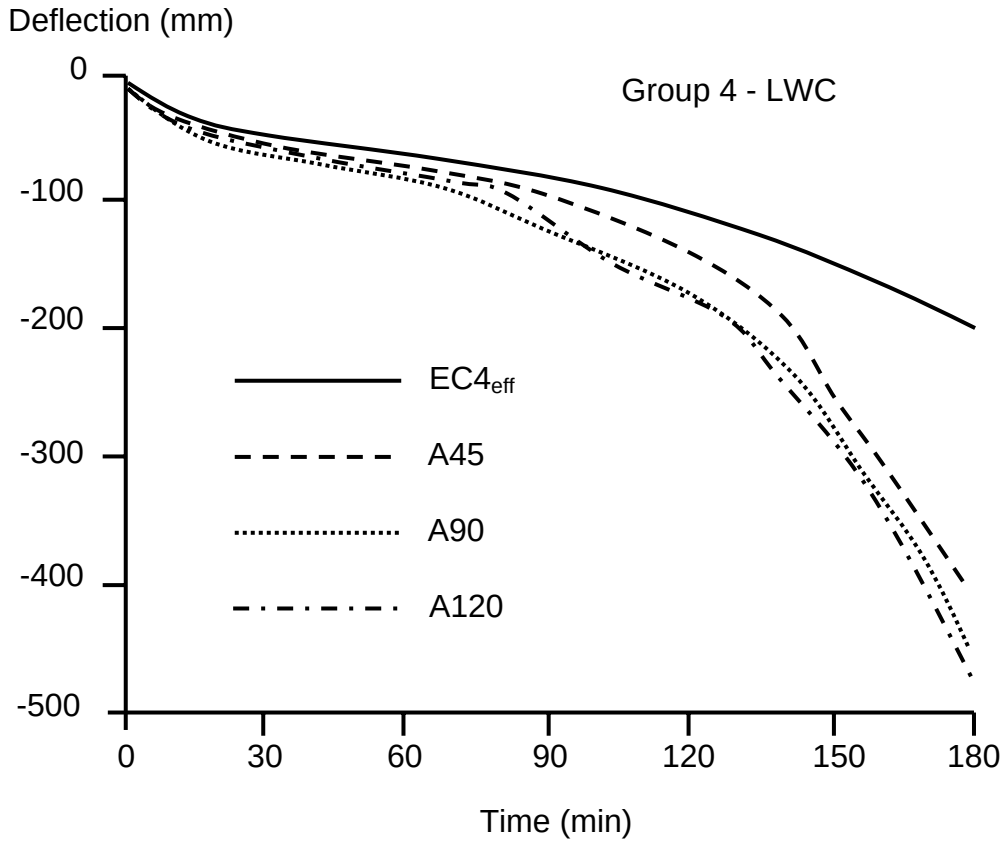
Deflection (mm)
0
-100
-200
-300
-400
-500
Group 4 - LWC
EC4eff
A45
A90
A120
0
30
60
90
120
150
180
Time (min)

Fig. 22 (d)

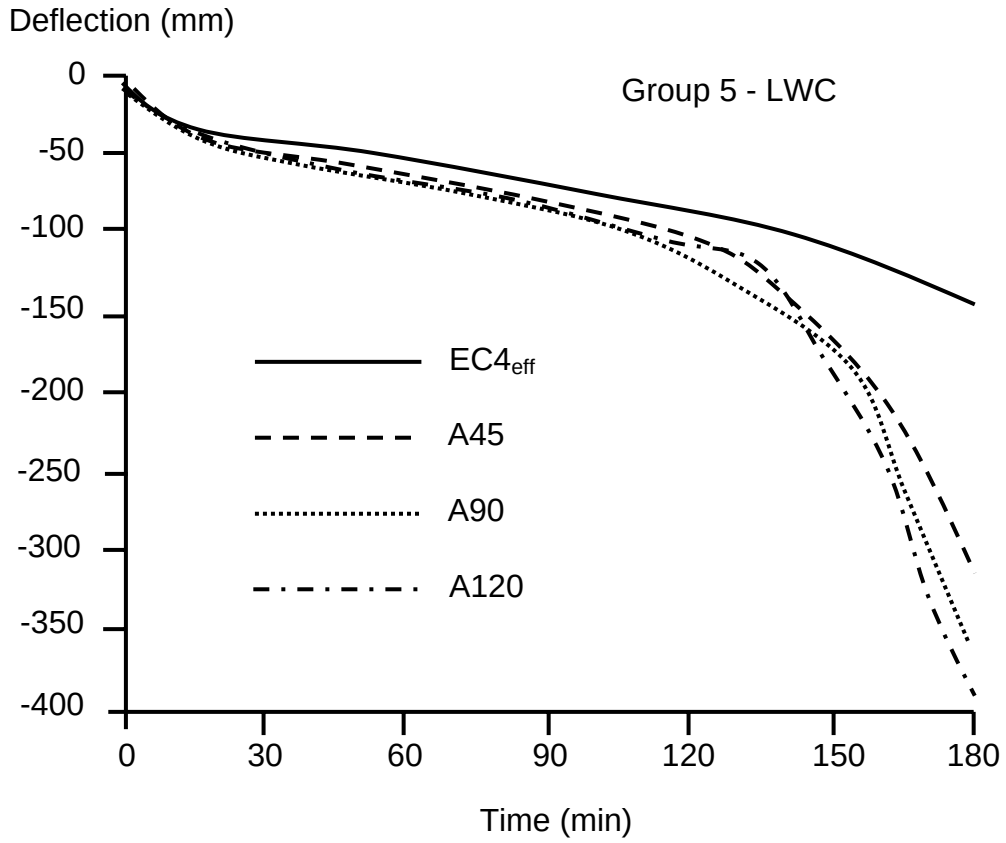
Deflection (mm)
0
-50
-100
-150
-200
-250
-300
-350
-400
Group 5 - LWC
EC4eff
A45
A90
A120
0
30
60
90
120
150
180
Time (min)

Fig. 22 (e)

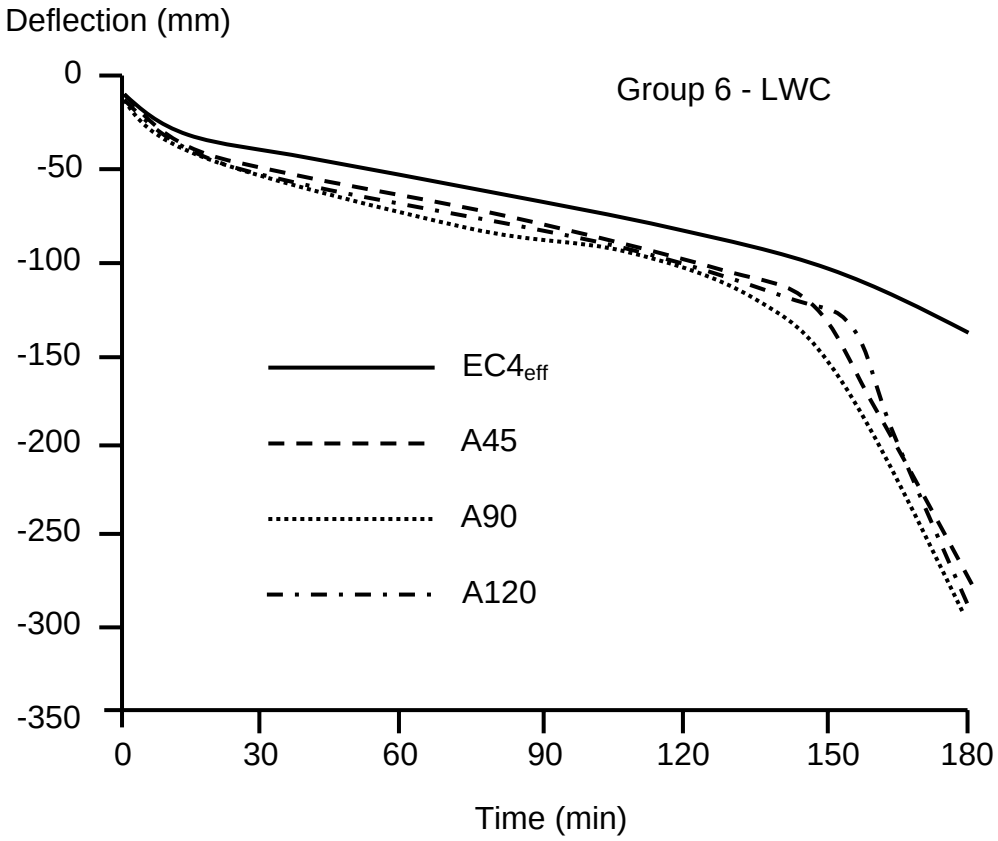
Deflection (mm)
0
-50
-100
-150
-200
-250
-300
-350
Group 6 - LWC
EC4eff
A45
A90
A120
0
30
60
90
120
150
180
Time (min)

Fig. 22 (f)

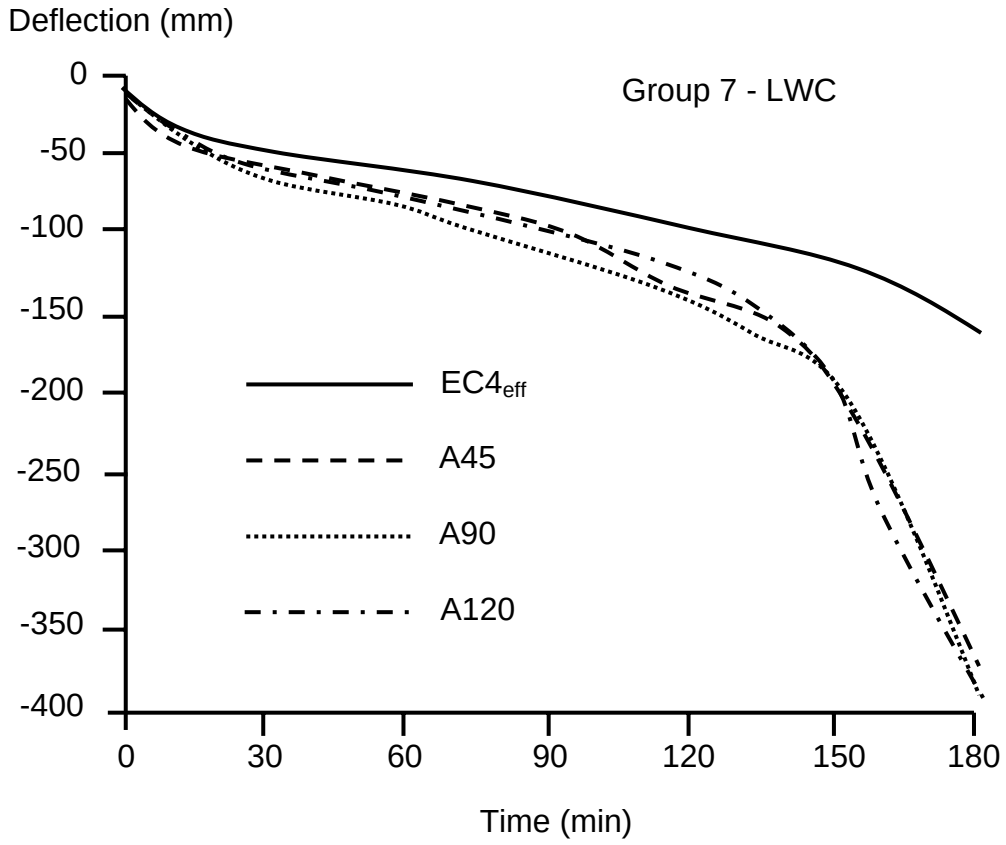
Deflection (mm)
0
-50
-100
-150
-200
-250
-300
-350
-400
Group 7 - LWC
EC4eff
A45
A90
A120
0
30
60
90
120
150
180
Time (min)

Fig. 22 (g)